

**MOLECULAR DYNAMICS SIMULATION OF  
MONTMORILLONITE AND MECHANICAL AND  
THERMODYNAMIC PROPERTIES CALCULATIONS**

A Thesis

by

SELMA ATILHAN

Submitted to the Office of Graduate Studies of  
Texas A&M University  
in partial fulfillment of the requirements for the degree of

MASTER OF SCIENCE

May 2007

Major Subject: Chemical Engineering

**MOLECULAR DYNAMICS SIMULATION OF  
MONTMORILLONITE AND MECHANICAL AND  
THERMODYNAMIC PROPERTIES CALCULATIONS**

A Thesis

by

SELMA ATILHAN

Submitted to the Office of Graduate Studies of  
Texas A&M University  
in partial fulfillment of the requirements for the degree of

MASTER OF SCIENCE

Approved by:

Chair of Committee,	Tahir Çağın
Committee Members,	Perla B. Balbuena
	Hung Jue Sue
Head of Department,	N.K. Anand

May 2007

Major Subject: Chemical Engineering

## ABSTRACT

Molecular Dynamics Simulation of Montmorillonite and Mechanical and  
Thermodynamic Properties Calculations. (May 2007)

Selma Atilhan, B.S., Ege University;

M.S., Ege University

Chair of Advisory Committee: Dr. Tahir Çağın

Nanocomposites refer to the materials in which the defining characteristic size of inclusions is in the order of 10-100nm. There are several types of nanoparticle inclusions with different structures: metal clusters, fullerenes particles and molybdenum selenide, Our research focus is on polymer nanocomposites with inorganic clay particles as inclusions, in particular we used sodium montmorillonite polymer nanocomposite.

In our study, modeling and simulations of sodium montmorillonite ( $\text{Na}^+$ -MMT) is currently being investigated as an inorganic nanocomposite material.  $\text{Na}^+$ -MMT clay consists of platelets, one nanometer thick with large lateral dimensions, which can be used to achieve efficient reinforcement of polymer matrices. This nanocomposite has different applications such as a binder of animal feed, a plasticizing agent in cement, brick and ceramic, and a thickener and stabilizer of latex and rubber adhesives.

In this study, sodium montmorillonite called  $\text{Na}^+$ -MMT structure is built with the bulk system and the layered system which includes from 1 to 12 layers by using Crystal Builder of Cerius<sup>2</sup>. An isothermal and isobaric ensemble is used for calculation of thermodynamic properties such as specific heat capacities and isothermal expansion coefficients of  $\text{Na}^+$ -MMT. A canonical ensemble which holds a fixed temperature, volume and number of molecules is used for defining exfoliation kinetics of layered structures and surface formation energies for  $\text{Na}^+$ -MMT layered structures are calculated by using a canonical ensemble. Mechanical properties are used to help characterize and identify the  $\text{Na}^+$ -MMT structure. Several elastic properties such as compliance and stiffness matrices, Young's, shear, and bulk modulus, volume compressibility, Poisson's ratios, Lamé constants, and velocities of sound are calculated in specified directions.

Another calculation method is the Vienna Ab-initio Simulation Package (VASP). VASP is a complex package for performing ab-initio quantum-mechanical calculations and molecular dynamic (MD) simulations using pseudopotentials and a plane wave basis set. Cut off energy is optimized for the unit cell of Na<sup>+</sup>-MMT by using different cut off energy values. Experimental and theoretical cell parameters are compared by using cell shape and volume optimization and root mean square (RMS) coordinate difference is calculated for variation of cell parameters. Cell shape and volume optimization are done for calculating optimum expansion or compression constant.

## **DEDICATION**

To my excellent husband, Mert and our families

## ACKNOWLEDGMENTS

I can hardly thank my advisor and the committee chair Dr. Çağın enough. He truly has been my role model and guided me in the right track of research and life too. I sincerely thank my committee members, Perla B. Balbuena and Hung Jue Sue, for serving on my committee.

I would like to express my appreciation to my group members, especially Mustafa Uludoğan, Arnab Chakrabarty and Oscar Ojeda, for valuable discussions, exchange of ideas and friendship.

I've been delighted to have such wonderful professors, colleagues, and friends here in College Station. Mr. Polasek's help regarding computer issues was truly invaluable.

Finally, I am forever grateful for the love and support of my parents and my husband. As teachers, my mother and father taught me the value of education. As parents, they instilled in me the importance of doing my best regardless of the circumstances. I am blessed to have them as parents and honored to have them as my role models. I want to thank my parents-in-law for their support and for giving their best wishes to us. Also I want to express my appreciation to my sister, brother, brothers-in-law and sisters-in-law for their support. Above all, I am indebted to my husband Mert for his love, support, encouragement, advice in hard times, and moreover, for the many sacrifices he made for the pursuit of my career ambitions. He truly is my foundation.

## NOMENCLATURE

$\alpha$ : Lattice angle between x and y directions

$\beta$ : Lattice angle between x and z directions

$\gamma$ : Lattice angle between y and z directions

a: Lattice parameter

b: Lattice parameter

c: Lattice parameter

$\xi$ : Atomic position on x direction

$\mu$ : Atomic position on y direction

$\zeta$ : Atomic position on z direction

## TABLE OF CONTENTS

	Page
ABSTRACT .....	iii
DEDICATION.....	v
ACKNOWLEDGMENTS .....	vi
NOMENCLATURE .....	vii
TABLE OF CONTENTS .....	viii
LIST OF FIGURES .....	x
LIST OF TABLES.....	x
 CHAPTER	
I INTRODUCTION.....	1
1.1 Definition of Nanocomposites.....	1
1.2 Structure and Chemical Formula of Clay .....	2
1.3 Montmorillonite.....	3
1.3.1 Montmorillonite and Its Physical Properties .....	3
1.3.2 Sodium Montmorillonite and Its Applications .....	4
1.4 Synthetic Methods for Polymer Layered Clay Nanocomposites.....	5
II THEORY .....	9
2.1 Introduction to Molecular Simulation .....	9
2.2 Molecular Dynamics.....	10
2.2.1 Force Fields.....	12
2.2.1.1 The Energy Expression .....	13
2.2.1.2 Advantages of Having Several Force Fields.....	13
2.2.1.3 Types of Force Field .....	14
2.2.1.3.1 Dreiding Force Field.....	16
2.2.1.3.2 Morse Charge Equilibration (MS-Q) Force Field.....	21
2.2.2 Ensembles .....	22
2.2.3 Types of Molecular Dynamics.....	23
2.3 Ab-Initio .....	25
2.3.1 Density Functional Theory .....	25
2.3.2 Advantages and Limitations of Ab-Initio Calculations .....	29



CHAPTER	Page
2.4 Properties from Simulation .....	30
2.5 A Survey of Earlier Work on Clay-Polymer Composites Literature Survey	34
III RESULTS AND DISCUSSIONS.....	36
3.1 Computational Details.....	36
3.1.1 Interaction Force Field: Functional Forms and Parameters Used In Simulations .....	36
3.1.2 Model Construction and Molecular Dynamics of MMT .....	38
3.2 Na <sup>+</sup> -MMT Bulk Structure (3x2x2) by Using NPT Molecular Dynamics.....	42
3.3 Different Layered Na <sup>+</sup> -MMT Structures.....	47
3.4 Na <sup>+</sup> -MMT Unit Cell (1x1x1) by Using NVT Molecular Dynamics .....	50
3.5 Exfoliation Studies on Organically Modified-MMT .....	56
3.6 VASP Calculations .....	58
IV CONCLUSION .....	62
REFERENCES .....	64
APPENDIX A.....	69
APPENDIX B .....	71
VITA.....	81

## LIST OF FIGURES

	Page
Fig. 1. Structure of 2:1 phyllosilicates [3] .....	2
Fig. 2. Polyhedra rendering of crystal structure of Na <sup>+</sup> -montmorillonite clay .....	3
Fig. 3. Schematic view of preparation methods for polymer intercalation compounds [7] .....	7
Fig. 4. Scheme of different types of composite arising from the interaction of polymers and layered nanocomposites[12].....	8
Fig. 5. Dreiding FF bonded and nonbonded interactions.....	18
Fig. 6. Schematic illustration of the self-consistent cycles in ab initio calculations .....	28
Fig. 7. Na <sup>+</sup> -MMT bulk structure .....	41
Fig. 8. MMT-NH <sub>3</sub> CH <sub>3</sub> .....	41
Fig. 9. Models of layered structures of Na <sup>+</sup> -MMT .....	41
Fig. 10. Total energy changes with respect to temperature for Na <sup>+</sup> -MMT bulk structure (3x2x2) by using NPT molecular dynamics .....	42
Fig. 11. Enthalpy changes with respect to pressure for Na <sup>+</sup> -MMT bulk structure (3x2x2) by using NPT molecular dynamics .....	43
Fig. 12. Pressure changes with respect to volume for Na <sup>+</sup> -MMT bulk structure (3x2x2) by using NPT molecular dynamics (compressibility calculation).....	43
Fig. 13. Compressibility changes with respect to temperature for Na <sup>+</sup> -MMT bulk structure (3x2x2) by using NPT molecular dynamics .....	44
Fig. 14. Volume changes with respect to temperature for Na <sup>+</sup> -MMT bulk structure (3x2x2) by using NPT molecular dynamics (thermal expansion coefficient calculation) .....	45
Fig. 15. Cell parameters changes with respect to temperature for Na <sup>+</sup> -MMT bulk structure (3x2x2) by using NPT molecular dynamics (linear thermal expansion coefficient calculation) .....	45

Fig. 16. Calculated required energy values for breaking off layers from the Na <sup>+</sup> -MMT structure as a function of one layer at different temperature .....	47
Fig. 17. Volume change with respect to temperature for different layered Na <sup>+</sup> -MMT structure (thermal expansion coefficient) .....	48
Fig. 18. Total energy changes with respect to temperature for different layered Na <sup>+</sup> -MMT structure (Cp calculation).....	49
Fig. 19. Bulk modulus changes with respect to pressure for Na <sup>+</sup> -MMT unit cell (1x1x1) by using NVT molecular dynamics at 300K .....	50
Fig. 20. Elastic constants changes with respect to pressure for Na <sup>+</sup> -MMT unit cell (1x1x1) by using NVT molecular dynamics at 300K .....	51
Fig. 21. Young's moduli changes with respect to pressure for Na <sup>+</sup> -MMT unit cell (1x1x1) by using NVT molecular dynamics at 300K .....	52
Fig. 22. Lamé constants changes with respect to pressure for Na <sup>+</sup> -MMT unit cell (1x1x1) by using NVT molecular dynamics at 300K .....	52
Fig. 23. Pressure changes with respect to volume for Na <sup>+</sup> -MMT unit cell (1x1x1) by using NVT molecular dynamics at 300K.....	53
Fig. 24. Annealing procedure for alkyl amine-MMT molecular dynamics .....	56
Fig. 25. Gallery height versus number of carbons n in the AA tail average at 300 <sup>0</sup> C.....	57
Fig. 26. Determination of cut off energy value for Na <sup>+</sup> -MMT unit cell (1x1x1) by using VASP .....	58
Fig. 27. Total energy changes for Na <sup>+</sup> -MMT unit cell (1x1x1) by using volume optimization method in VASP .....	60
Fig. 28. Pressure and total energy changes for Na <sup>+</sup> -MMT unit cell (1x1x1) during volume optimization in VASP.....	61

## LIST OF TABLES

	Page
Table 1. Montmorillonite clay properties .....	4
Table 2. Types of ensembles.....	24
Table 3. Diagonal Morse type Van der Waals potential.....	37
Table 4. Off-diagonal Morse type Van der Waals potential.....	38
Table 5. Lattice parameters of Na-montmorillonite [49].....	38
Table 6. Na <sup>+</sup> -montmorillonite atomic coordinates [48, 49].....	40
Table 7. Thermodynamic properties of Na <sup>+</sup> -MMT.....	46
Table 8. Mechanical properties calculated by using Cerius2 of Na <sup>+</sup> -MMT unit cell (1x1x1) at 300K.....	55
Table 9. Mechanical properties calculated by using Cerius2 of Na <sup>+</sup> -MMT unit cell (1x1x1) at 300K (continued) .....	56
Table 10. Gallery height changes with respect to various number of carbon atoms and various anneal cycles.....	57
Table 11. Na <sup>+</sup> -MMT unit cell shape and volume optimization .....	59
Table 12. Optimization of cell parameter c and RMS results for Na <sup>+</sup> -MMT unit cell (1x1x1) by using volume optimization method in VASP.....	61

# CHAPTER I

## INTRODUCTION

### 1.1 Definition of Nanocomposites

The material systems described as nanocomposites getting richer day by day over a range of systems with one, two and three dimensional nanoscale composites in various matrix materials such as metals, ceramics and polymers.

Inorganic-polymer nanocomposites are composites with inorganic materials as inclusions. The inorganic components can be a three-dimensional framework systems such as feldspar group (albite, microcline), feldspathoid group (cancrinite, leucite, sodalite), quartz group (coesite, quartz, tridymite) and zeolite group (analcime, mesolite, phillipsite), two-dimensional layered materials such as clays (kaolinite, montmorillonite/smectite, clay-mica and chlorite groups), metal oxides ( $V_2O_5$  xerogel and aerogel), silicates (aluminum silicates, magnesium silicates, magnesium iron silicates, zirconium silicates, potassium magnesium aluminum silicate hydroxide fluorides), n-silicates, metal phosphates, and even one-dimensional such as nanowire, nanorod, nanotube and zero-dimensional materials such as  $(Mo_3Se_3)^-$ , fullerene particles and clusters. Experiments indicate that essentially all types and classes of nanocomposite materials lead to new and enhanced properties when compared to their macrocomposite analogues. Consequently, nanocomposites have potential new applications in several areas such as mechanically reinforced light-weight components (Concrete, Carbon-fiber-reinforced plastics), non-linear optics (metal and semiconductor nanocomposites (copper, silver nanoparticles,  $\beta$ -BaB<sub>2</sub>O<sub>4</sub>, LiB<sub>3</sub>O<sub>5</sub>)), nanosensors (chemical nanosensors used on multi wall carbon nanotubes, devices and methods for detection of basic gases and thermal nanosensors used for temperature control, fire detection, engine environment monitoring (coolant and lubricant temperatures)), battery cathodes ( $V_2O_5$ ,  $V_6O_{13}$ ), nanowires.

## 1.2 Structure and Chemical Formula of Clay

Clay is a natural, earthy, fine-grained material that develops plasticity when mixed with a limited amount of water. The most common clay minerals can be classified into five groups: smectite (montmorillonite, beidellite); illite (illite and glauconite); kaolinite (kaolinite, halloysite); chlorite (chlorite); sepolite (sepolite and palygorskite) [1].

Structurally, clays are built up of layers of octahedral and tetrahedral sheets. The primary building blocks of these sheets are the aluminum octahedron and the silica tetrahedron. The  $\text{Al}^{3+}$  is generally found in six fold or octahedral coordination while the  $\text{Si}^{4+}$  cation takes place in four fold or tetrahedral coordination with oxygen [1]. Layered silicates is a member of the 2:1 phyllosilicates structural family, in which the central octahedral alumina sheet is sandwiched between two tetrahedral silica sheets [2] (Fig. 1). These layered crystals, which are approximately 1nm thick with lateral dimensions from 30nm to several microns, are piled parallel to each other and are bonded by local van der Waals and electrostatic forces.

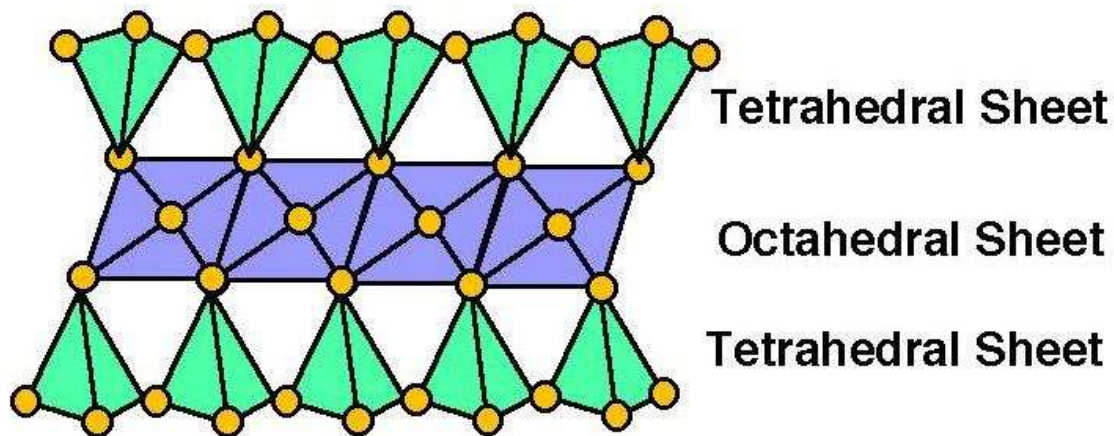


**Fig. 1.** Structure of 2:1 phyllosilicates [3]

Clays are naturally occurring minerals; they must be purified before use. The most commonly encountered layered silicates are montmorillonite, hectorite and saponite. The clay layers allow delocalization of negative charges. These negative charges are then neutralized by cations such as  $\text{H}^+$ ,  $\text{Na}^+$ ,  $\text{K}^+$ ,  $\text{Mg}^{2+}$  or  $\text{Ca}^{2+}$  situated in

between the charged layers. Because of their high hydrophilic nature, water molecules generally position between the clay layers [1, 2] as well.

### 1.3 Montmorillonite

#### 1.3.1 Montmorillonite and Its Physical Properties

Montmorillonite (MMT) is a well known clay mineral. The name derives from the French town Montmorillon, where it was discovered by Damour and Salvétat in 1847. MMT is formed by weathering of eruptive rock material (usually tuffs and volcanic ash). In its pure form, MMT includes trace amounts of cristobalite, zeolites, biotite, quartz, feldspar, zirconia, as well as some other minerals found in volcanic rocks [1]. MMT has a crystallographic structure based on pyrophyllite model. Pyrophyllite model structure consists of two silica tetrahedral sheets sandwiching an edge-shared octahedral sheet of either aluminum or magnesium hydroxide, known as t-o-t sheets. A polyhedra representation of MMT crystal structure is given in Fig. 2.

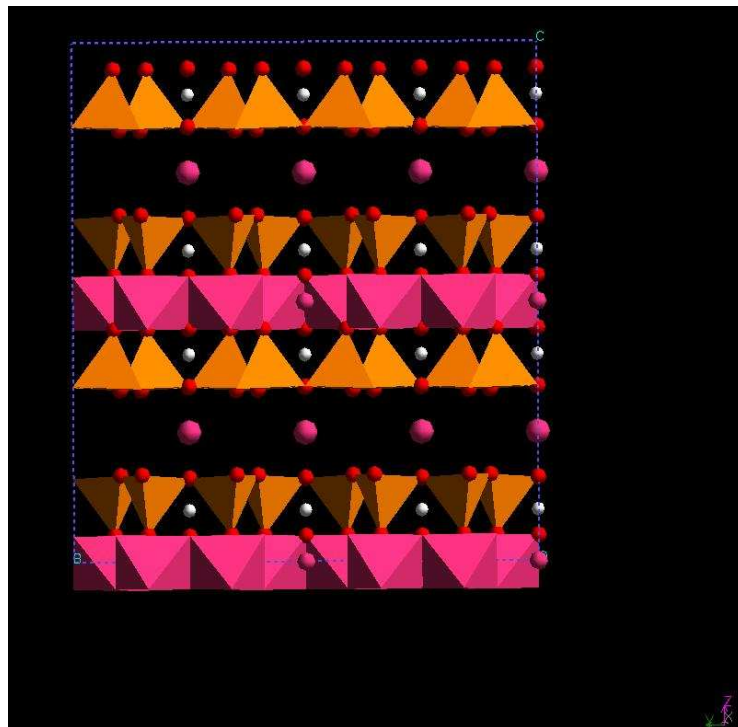


**Fig. 2.** Polyhedra rendering of crystal structure of  $\text{Na}^+$ -montmorillonite clay

MMT has the ability to absorb certain cations and to retain them in an exchangeable state which makes intercalated cations to be exchanged by other cations in a water solution.  $\text{Na}^+$  and  $\text{Ca}^{2+}$  are the most common exchangeable cations. Cation exchange capacity is constant for any given clay [1]. MMTs can be classified into two main parts as sodium MMT ( $\text{Na}^+$ -MMT) and calcium MMT ( $\text{Ca}^{2+}$ -MMT). Montmorillonite clay properties are shown in Table 1 [4].

**Table 1.** Montmorillonite clay properties

Class	Silicates
Subclass	Phyllosilicates
Crystal System	Monoclinic, C2/m
Member of	Smectite group
Color	White, yellow
Cleavage	Perfect in one direction, basal
Fracture	Uneven to lamellar
Luster	Earthy (dull)
Specific surface	800m <sup>2</sup> /g
Particle dimensions	From 0.1-1µm in length and 0.9nm in thickness
Mohs Hardness @20°C	1.5- 2.0
Average Specific Gravity (g/cc)	2.3- 3
Molecular Weight (g/mol.)	540.46
Average Density (g/cm <sup>3</sup> )	2.35
Characteristic	Crystals expand to many times their volume when added to water
Field Indicators	Softness, and soapy feel

### ***1.3.2 Sodium Montmorillonite and Its Applications***

$\text{Na}^+$ -MMT or with its commonly known name bentonite is a commonly and highly utilized industrial clay; which was first discovered in Fort Benton, Wyoming USA [5].  $\text{Na}^+$ -MMT has very small micron sized particles with extremely fine-grained and



thin-layered structure. Within these thin layers loosely bonded  $\text{Na}^+$  cations present. Loosely bonded  $\text{Na}^+$  cations are bound to one another and they are easily exchangeable.

$\text{Na}^+$ -MMT is the most developed and commercialized clay.  $\text{Na}^+$ -MMT is naturally hydrophilic and it has pretty good water affinity. Due to this property, they are incompatible with most polymers. Consequently it is difficult to get good mixing and dispersion of  $\text{Na}^+$ -MMT with polymer solutions. Additionally, the high electrostatic forces cause clay platelets to hold together tight [6]. For these reasons the clay must be treated so it can be incorporated into a polymer. In order to make clay surface more compatible with a polymer, ion exchanging method is a common application. On the other hand ion dipole interaction is an alternative method to ion exchanging method. As mentioned above, since the cations on the clay surface are loosely bound, they can be replaced by other cations. This process makes clay more hydrophobic and helps clay platelets to separate. When clay platelets are separated, they can be easily intercalated and then subsequently exfoliated into the polymer [6].

$\text{Na}^+$ -MMT clays have several application areas. To list of them:

- Binder of fodder (animal feeds) in pellet form.
- Binder of insulating material containing rock wool or asbestos fibers which are used in furnaces and steam boilers.
- Plasticizing agent in cement and grout.
- Plasticizer in brick, sewer pipe, ceramic, and refractory mixes.
- Thickener of fire retardant slurries dropped from aircraft.
- Thickener and stabilizer of latex and of rubber adhesives.
- Thickening, suspending, and adsorptive ingredient in medicines, pharmaceuticals, and cosmetics.
- Gelling agent in greases and lubricants.

#### **1.4 Synthetic Methods for Polymer Layered Clay Nanocomposites**

Intercalation of polymers into inorganic layered materials with retention of the layered structure is an excellent way of constructing novel inorganic-polymer composite systems. Fig. 3 shows a schematic view of intercalation reactions of polymers into the interlayer spaces. Intercalation is either done directly or done by in situ polymerization of pre-

intercalated monomers between the layers of host materials. Since direct intercalation is limited, preintercalated monomers becomes more important. However, control of molecular weight of the polymers become more difficult in situ polymerization method [7].

There are four main processes in preparing the polymer-layered silicate nanocomposites [8].

- ❑ *Exfoliation-adsorption*: By the assistance of a solvent in which polymer is soluble, layered silicate is exfoliated into layers. Some layered silicates can be easily dispersed in an adequate solvent due to the presence of weak forces between the layers. The polymer then adsorbs onto the delaminated sheets and when the solvent is evaporated (or the mixture precipitated), the sheets reassemble, sandwiching the polymer to form, in the best case, an ordered multilayer structure. In this process, nanocomposites are obtained by the emulsion polymerization while layered silicate is dispersed in the aqueous phase.
- ❑ *In situ intercalative polymerization*: In order to provide ground for polymer formation in between the intercalated sheets, layered silicate is swollen within the liquid monomer or monomer solution. Initiation of the polymerization process is given by heat or by the diffusion of a suitable initiator. Often organic initiator catalysts are used.
- ❑ *Melt intercalation*: Polymer is mixed with the layered silicate in molten state conditions. If the chosen polymer is compatible with the layered surfaces, the polymer can crawl into the interlayer space and form either an intercalated or an exfoliated nanocomposite. Solvent presence is not required for this process.
- ❑ *Template synthesis*: Double-layer hydroxide-based nanocomposites are synthesized by using silicate building blocks. These silicates are formed in situ in an aqueous solution containing the polymer [9, 10]. In this technique, the polymer aids the nucleation and growth of the inorganic host crystals and gets trapped within the layers as they grow based on self-assembly forces [11].

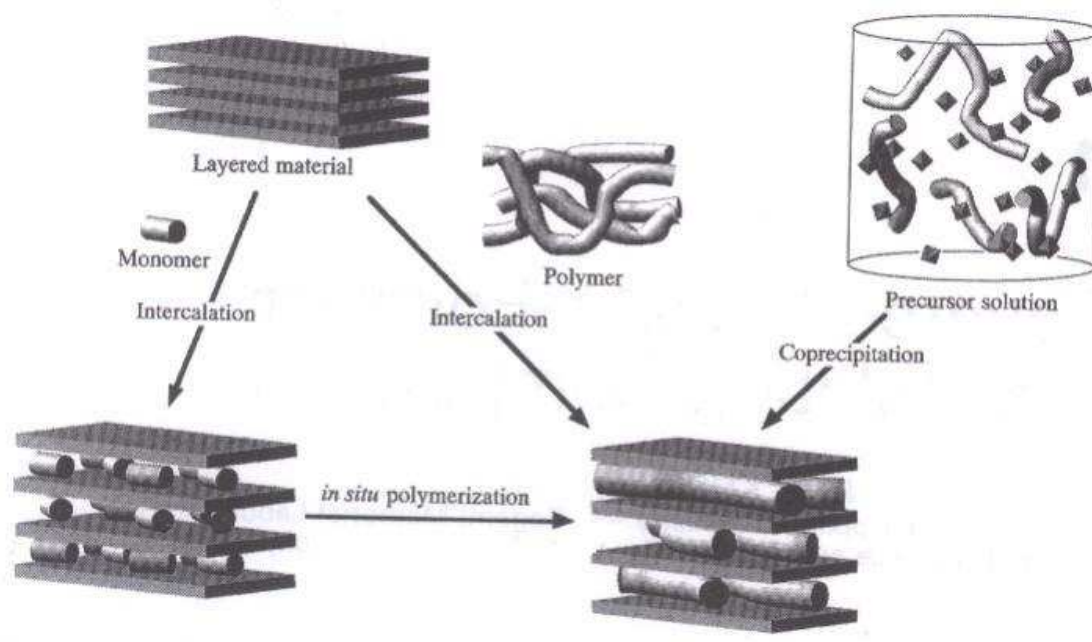


**Fig. 3.** Schematic view of preparation methods for polymer intercalation compounds [7]

Depending on the interaction between the layered clay and the nature of the surfactant, different types of nanocomposites, ranging from immiscible to exfoliated, can be obtained, as shown in Fig. 4. In conventional or immiscible composites, the polymer chains are unable to penetrate between the clay layers; in intercalated nanocomposite, one or more polymer chains intercalate between the clay layers, but the registry between the clay layers is maintained; in exfoliated nanocomposite, the registry between the clay layers is lost, the clay layers are completely delaminated and the individual clay layers can be seen [2]. Dispersing clays in polymers is important to obtain complete delamination of the clay in the matrix polymer. This has become possible due to the recent advances [2].

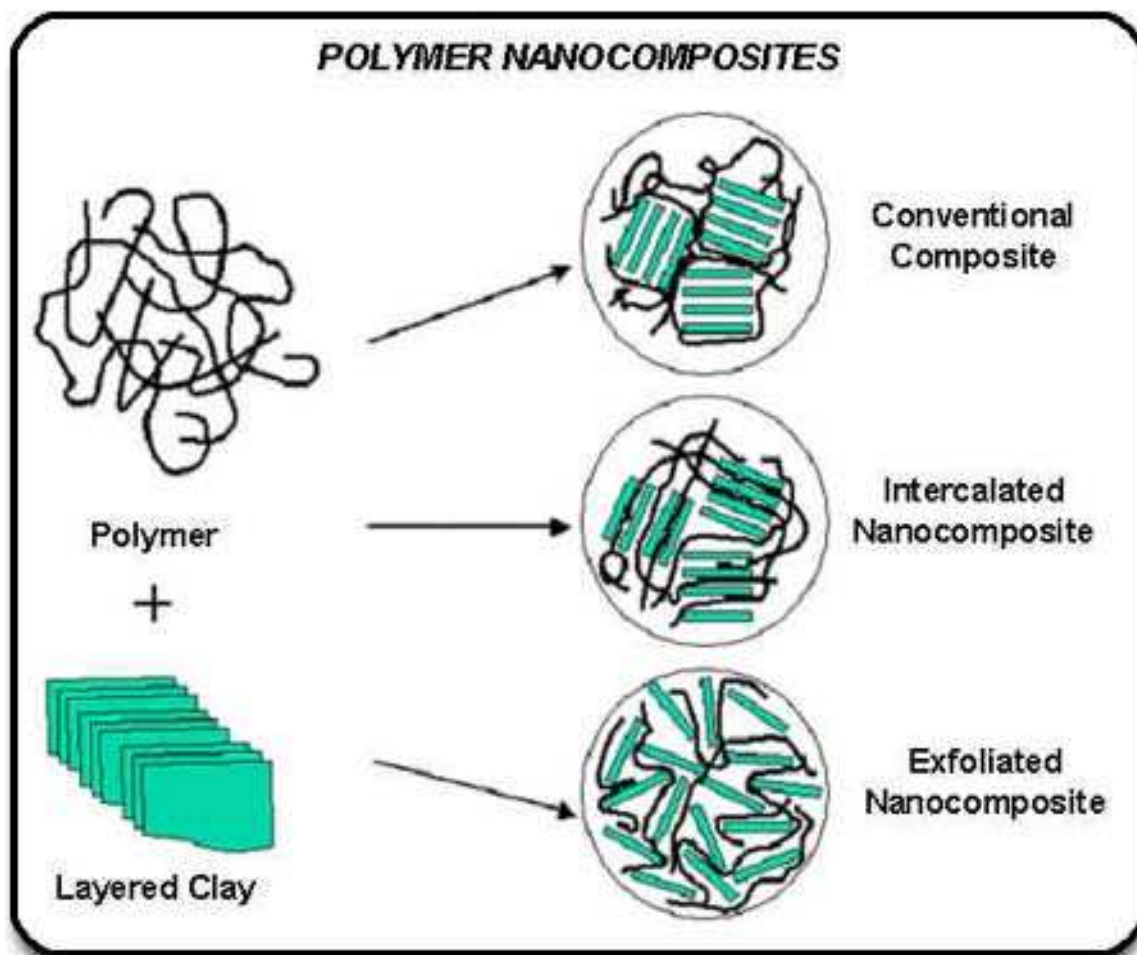


**Fig. 4.** Scheme of different types of composite arising from the interaction of polymers and layered nanocomposites[12]

## CHAPTER II

### THEORY

#### 2.1 Introduction to Molecular Simulation

After the end of 2<sup>nd</sup> World War, the use of computers and associated computational methods in solving problems in science and engineering have grown dramatically and leading to emerging fields such as computational physics, computational chemistry, computational fluid dynamics, computational solid mechanics, etc. as the computational methods become feasible [1, 2, 13-15]. As the high performance computers with increasing efficiency become available, scientists and engineers are handling modeling and simulations approaches to problems using levels of methods ranging from quantum level calculations to chemical plant design. In this study, we shall focus our attention only on the atomic or molecular scale simulations, which covers the time scale up to a few tens of nano-seconds and the length scale up to a few tens of nanometers.

Molecular simulations play a crucial role especially in nanoscale research due to compatible nature of length and time scales involved. In general, one may use molecular simulation approaches to compare the calculated properties of systems with the experimental results. But even more important, molecular simulations can be employed to the systems that have not been studied via experiments [13, 15] in order to aid or guide the development of new material systems and structures. This, of course, requires enhancing the predictive power of molecular simulations. In classical molecular simulations this requires improvement of the functional form and parameterization of the intermolecular and intramolecular interactions underlying the physics and chemistry of the materials systems. The functional forms and associated parameters, i.e. the force-fields, may be improved by validating the simulation results against the experiments. With reliable interaction force fields, molecular simulations can be used to guide the physical experiments. Furthermore, molecular simulations served as a test method for new theories of condensed phases of matter by theoreticians. That is to say, in this case simulations may be used to screen the theories and play the role of testing by experiments. Therefore, we may refer to a molecular simulation processes as *computer*

*'virtual' experiments* [13]. Molecular dynamics (MD) simulation and Monte Carlo (MC) simulation are the two basic techniques in the molecular simulation world.

Through molecular simulations with reliable interaction force fields, the macroscopic thermodynamic properties such as pressure, internal energy, thermal expansion, compressibility, tensile and shear modulus, specific heats can be evaluated by using the microscopic level information generated through simulations [15]. For instance, the equilibrium macroscopic properties are calculated by taking the averages or time averages in molecular dynamics,, and ensemble averages in Monte Carlo simulations. On the other hand, transport macroscopic properties - often referred as dynamic properties-, can be measured from molecular dynamics simulation using appropriate time correlation functions of the relevant microscopic variables over the generated time series -trajectory.

## **2.2 Molecular Dynamics**

Molecular dynamics first introduced by Alder and Wainwright [16], in order to study the condensed phase of fluids beyond the gas state densities. Early simulations utilized hard core representation for interactions, In 1964 Rahman [17] carried out first simulation including long range interactions (soft sphere) by employing Lennard-Jones potential to represent the interactions in liquid argon as opposed to hard sphere . Since then the molecular dynamics simulations with continuous potentials became a very widely used research tool for researcher to calculate the bulk properties of materials and to develop fundamental physical understanding of systems including complex systems such as biological and synthetic polymers.

The theoretical basis in using molecular modeling in relating atomistic trajectories in space to macroscopic physico-chemical properties is statistical thermodynamics. Hence, through determining the structure and dynamics of a system at the atomistic level one can predict the bulk property of a system at the macroscopic level. One approach to establish this connection is through molecular dynamics (MD). MD generates information at the atomistic level by producing a time series of positions and momenta of these particles through which one can determine the physical properties. The time series for position and momenta –trajectory – is obtain via solving the Newtonian equations of motion for an N-body system.

The equations of motion is simply the statement of Newton's second law for each particle in N-body systems,

$$\text{Force} = \text{mass} * \text{acceleration} \text{ or } F_i = m_i * a_i, (1)$$

Here the force on a given particle is a function of the coordinates of the other particles in the N-body system. Hence the equations of motion are iteratively solved in time as the positions and velocities of particles change. The force on any atom is calculated from the derivative of energy at each configuration –for a system under no external force:

$$-\frac{dE}{dr_i} = F_i (2)$$

One may evaluate the energies and forces using a classical force fields or a selected level of quantum theory. In practice, the atoms are assigned initial velocities that conform to the total kinetic energy of the system, which in turn, is dictated by the desired simulation temperature. From the knowledge of the force on each atom, it is possible to determine the acceleration of each atom in the system. Integration of the equations of motion then yields a trajectory that describes the positions, velocities and accelerations of the particles as they vary with time. From this trajectory, the average values of properties can be determined. The method is deterministic; once the positions and velocities of each atom are known, the state of the system can be predicted at any time in the future or the past. Molecular dynamics simulations can be time consuming and computationally expensive. However, computers are getting faster and cheaper. Simulations of solvated proteins are calculated up to the nanosecond time scale; however, simulations into the millisecond regime have been reported.

Identification and evaluation of different type of interactions between different types of particles is expressed through what we call the force fields. There are many types of force field. We will describe some of the widely used force fields below. In our calculations we have used a force field which accurately represents the interactions within clay and interactions with organic molecules and polymers and within organic polymers.

### 2.2.1 Force Fields

The functional form of the potential energy expression and the entire set of parameters needed to fit the potential energy surface constitute the force field. The energy expression is the specific equation that is set up for a particular model (types of atoms, particular connectivity, choices for attributes, etc) and including (or not) any optional terms.

It is important to understand that the force field both the functional form and the parameters themselves represents the single largest approximation in molecular modeling. The quality of the force field, its applicability to the model at hand, and its ability to predict the particular properties measured in the simulation directly determine the validity of the results.

The force field contains the necessary building blocks for the calculations of energy and force:

- ❖ A list of atom types.
- ❖ A list of atomic charges (if not included in the atom-type information).
- ❖ Atom-typing rules.
- ❖ Functional forms for the components of the energy expression.
- ❖ Parameters for the function terms.
- ❖ For some force fields, this may include some rules for generating parameters that have not been explicitly defined.
- ❖ For some force fields, this may include a specified way of assigning the functional forms and associated parameters.

The force fields commonly used for describing molecules, polymers, biopolymers usually employ a combination of internal coordinates and terms (bond distances, bond angles, torsions, etc.), to describe part of the potential energy surface due to interactions between bonded atoms, and nonbond terms to describe the van der Waals and electrostatic interactions between atoms. The functional forms range from simple quadratic forms to Morse functions, Fourier expansions, Lennard–Jones potentials, etc.

The goal of a force field is to describe entire classes of molecules with reasonable accuracy. In a sense, the force field interpolates and extrapolates from the empirical data of the small set of models used to parameterize the force field to a larger set of related



models. Some force fields aim for high accuracy for a limited set of element types, thus enabling good prediction of many molecular properties. Other force fields aim for the broadest possible coverage of the periodic table, with necessarily lower accuracy.

### 2.2.1.1 The Energy Expression

The actual coordinates of a model combined with the force field data create the energy expression (or target function) for the model. This energy expression is the equation that describes the potential energy surface of a particular model as a function of its atomic coordinates. The potential energy of a system can be expressed as a sum of valence (or bond), and nonbonded interactions.

The energy of valence interactions is generally accounted for by diagonal terms, namely, bond stretching ( $E_{\text{bond}}$ ), valence angle bending ( $E_{\text{angle}}$ ), dihedral angle torsion ( $E_{\text{torsion}}$ ), and inversion ( $E_{\text{inversion}}$ ) terms, which are part of nearly all force fields for covalent systems.

$$E_{\text{val}} = E_{\text{bond}} + E_{\text{angle}} + E_{\text{torsion}} + E_{\text{inv}} \quad (3)$$

The energy of interactions between nonbonded atoms is accounted for by van der Waals ( $E_{\text{vdW}}$ ), electrostatic ( $E_{\text{Coulomb}}$ ), and (in some older force fields) hydrogen bond ( $E_{\text{hbond}}$ ) terms:

$$E_{\text{nonbond}} = E_{\text{vdW}} + E_{\text{Coulomb}} + E_{\text{hbond}} \quad (4)$$

### 2.2.1.2 Advantages of Having Several Force Fields

A broader range of systems can be treated: Some classical force fields were originally created for modeling proteins and peptides, others for DNA and RNA. Some have been extended to handle more general systems having similar functional groups. The rule-based force fields have extended the range of force field simulations to a broader range of elements. The second-generation force fields currently include parameters for all functional groups appropriate for protein simulations.

Identical calculations with two or more independent force fields can be compared to assess the dependence of the results on the force field: For example, amino acid parameters are defined in the AMBER, CHARMM, CVFF, CFF, and MMFF94 force

fields, so peptide and protein calculations with these force fields can be compared to assess the effect of the force fields.

The different functional forms used in the various energy expressions increase the flexibility of molecular mechanics or molecular dynamics program: You can balance the requirements of high accuracy vs. available computational resources. (Highly accurate force fields are generally more complex and therefore require more resources.) Different energy terms can be compared. For example, approximations such as a distance-dependent dielectric constant or scaling of 1–4 nonbond interactions can be assessed. Harmonic bond terms are accurate only at bond lengths close to the reference bond length, but the Morse term can be used to model bond breaking.

The development of new force fields and elsewhere continues to provide more accurate and more broadly applicable force fields. As experience is gained in parameterizing the force fields and as new experimental data become available, the range of both properties and systems fit by these newer force fields will increase.

### 2.2.1.3 Types of Force Field

Many different force fields which are suitable for systems dealt in this thesis exists, such as CHARMM, AMBER, Dreiding, CFF, PCFF, Universal, CVFF. These are some of the most frequently used force fields. Based upon need and target system it's a referred practice to modify an existing force field in order to get the best values out of it. Sometimes one may also go to an extent to develop a separate force field to suit the needs of the specific research.

Force fields are classified in different classes. There are second generation force fields developed by high parameterization (examples CFF, PCFF COMPASS etc), rule based force fields like Universal and Dreiding where parameters are decided by some rules (example hybridization), classical or first generation force field like AMBER, CHARMM and CVFF which is also based on parameterization but mostly from experimental values as oppose to that of second generation which is based on quantum input and special purpose force field.

**CVFF force field** is also based on parameterization but mostly from experimental values as oppose to that of second generation which is based on quantum input and

special purpose force field. CVFF includes harmonic bond stretching and bond angle bending terms, a shifted 12-6 Lennard Jones potential for nonbonded interactions, and a Coulombic term for interactions between atom-centered partial atomic charges [18].

$$E_{pot} = \sum_b k_b (b - b_0)^2 + \sum_\theta k_\theta (\theta - \theta_0)^2 + \sum_\phi k_\phi [1 + s \cos(n\phi)] + \sum_{i,j} \epsilon \left[ \left( \frac{A}{r_{ij}} \right)^{12} - \left( \frac{B}{r_{ij}} \right)^6 \right] + \sum_{i,j} \frac{q_i q_j}{\epsilon r_{ij}} \quad (5)$$

where  $k_b$ ,  $k_\theta$ ,  $k_\phi$  are force constants,  $n$  is multiplicity and  $\Phi$  is the phase angle for the torsional angle parameters. The  $A$ ,  $B$ , and  $q$  parameters are the nonbonded potentials.

**AMBER force field** is widely used for simulation of proteins and nucleic acids [19]. First term of Eq 6 (summing over bonds) represents the energy between covalently bonded atoms. This harmonic (ideal spring) force is a good approximation near the equilibrium bond length, but becomes increasingly poor as atoms separate. Second term (summing over angles): represents the energy due to the geometry of electron orbitals involved in covalent bonding. Third term (summing over torsions): represents the energy for twisting a bond due to bond order (e.g. double bonds) and neighboring bonds or lone pairs of electrons. Note that a single bond may have more than one of these terms, such that the total torsional energy is expressed as a Fourier series. Fourth term (double summation over  $i$  and  $j$ ): represents the non-bonded energy between all atom pairs, which can be decomposed into van der Waals (first term of summation) and electrostatic (second term of summation) energies. The form of the electrostatic energy used here assumes that the charges due to the protons and electrons in an atom can be represented by a single point charge. (Or in the case of parameter sets that employ lone pairs, a small number of point charges.)

$$E_{pot} = \sum_b \frac{1}{2} k_b (l - l_0)^2 + \sum_\theta \frac{1}{2} k_\theta (\theta - \theta_0)^2 + \sum_\phi \frac{V_n}{2} k_\phi [1 + \cos(n\phi - \gamma)] + \sum_{i,j} \left[ \left( \frac{A}{r_{ij}} \right)^{12} - \left( \frac{B}{r_{ij}} \right)^6 \right] + \sum_{i,j} \frac{q_i q_j}{\epsilon r_{ij}} \quad (6)$$

In Eq 6,  $k_b$ ,  $k_\theta$ ,  $k_\phi$  are force constants,  $n$  is multiplicity and  $\Phi$  is the phase angle for the torsional angle parameters. The  $A$ ,  $B$ , and  $q$  parameters characterize the nonbonded potentials.

**CHARMM** (a general and flexible software application for modeling program for studying the structure and behavior of molecular systems ranging from an individual

organic molecule to large proteins in its solvent environment) uses similar energy functions as the others with parameterized extensively using empirical data for energy minimization, molecular dynamics simulation, or vibrational analysis. In these specialized force fields, there are often understated differences in force constants and geometric parameters for similar atoms in slightly different environments, and it is often not clear how to generalize for new atoms or new bond types.

$$E_{\text{Bond}} = k_l (l - l_o)^2 \quad (7)$$

$$E_{\text{angle}} = k_\theta (\theta - \theta_o)^2 \quad (8)$$

$$E_{\text{rotate}} = k_\phi [1 - \cos(n_{JK} \Phi)] \quad (9)$$

$$E_{\text{vdW}} = \sum 4\epsilon \left[ \left( \frac{\sigma_{ij}}{R_{ij}} \right)^{12} - \left( \frac{\sigma_{ij}}{R_{ij}} \right)^6 \right] \quad (10)$$

There are cases for reliable molecular modeling the first steps to be pursued is the development of a force field that contains parameters characterize the interactions more accurately than the existing force field models. In the present work we employ this kind of a force fields to represent the interactions between clay particles and polymers: In particular we employ the Morse-Stretch Charge Equilibration Force Field (MSQ) for the interactions within inorganic components [20] and supplement it with the Dreiding Force Field type for the interactions within the organic component [21]. The mixed non-bond organic-inorganic interactions (electrostatic and van der Waals) are separately calculated and added. One of the important features of these force fields is that the atomic charges are allowed to readjust instantaneously to the atomic configurations. These charges are calculated using the charge equilibration (QEQ) method [22].

### 2.2.1.3.1 Dreiding Force Field [21]

The source of the force field used for the organic interactions is a widely used force field known as Dreiding [21]. This force field was chosen because property predicted for polymer systems using this force field has given good agreement with the experimental values in the past [23, 24]. Just like any other force fields attempting to describe organics, Dreiding also employs different functions for describing the interaction energy. The energy of a system can be written as the sum of two components

and each component has multiple contributions deriving from the topology of organics molecules involved. Below, we give a summary of these terms:

$$E = E_{\text{VAL}} + E_{\text{NB}} \text{ where (11)}$$

$$E_{\text{VAL}} = E_{\text{B}} + E_{\text{A}} + E_{\text{T}} + E_{\text{I}} \text{ (12)}$$

$$E_{\text{NB}} = E_{\text{VDW}} + E_{\text{Coul}} + E_{\text{HB}} \text{ (13)}$$

$E_{\text{B}}$  = Energy due to Bond stretching (two body)

$E_{\text{A}}$  = Energy due to angle bending (three body)

$E_{\text{T}}$  = Energy due to torsion (four body)

$E_{\text{I}}$  = Energy due to out of plane configuration (four body)

$E_{\text{VDW}}$  = Energy due to van der Waals interaction

$E_{\text{Coul}}$  = Energy due to columbic interaction

$E_{\text{HB}}$  = Energy due to hydrogen bonding

The first four terms are due to bonded interaction the last two terms are due to nonbonded interactions (Fig. 5). All these terms will be discussed in little more detail in the following sections. It is this calculation of electrostatic interaction terms takes most of the simulation time. The simple reason being as this interaction can happen between any two atoms, ideally this calculation should be carried out for each atom and hence it takes time in the order of  $N^2$  where  $N$  is the number of atoms of the system. These interactions are also called long range interactions as they die out inversely with the value of 'r' and hence contributes some value till a large value of 'r'. Algorithms have been developed for handling the problem in such a way so that simulation time can be decreased without sacrificing the accuracy of the results as such. While length of simulation is one important aspect the other one is the time step used for the simulation. Ideally the time step in a simulation should be such that it can capture the fastest motion in the system which is typically the vibration mode. Typically time step in the order of 0.1 fs to 10 fs are used depending upon the system involved in the simulation. Sometimes in simulation the fastest parts are treated as constant and this enables one to take a longer time step and hence accelerating the whole process.

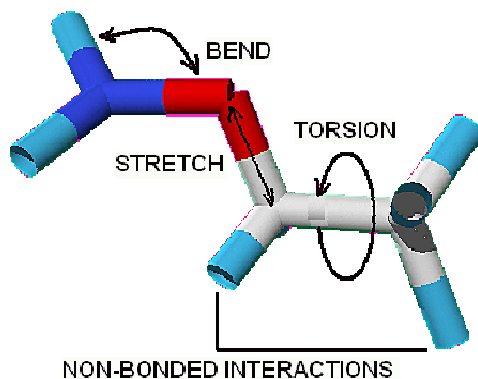


**Fig. 5.** Dreiding FF bonded and nonbonded interactions

- **Bond Stretch:** The first term in energy expression for bonded expression describes the change in energy associated with the change in bond length from the equilibrium value. It is assumed that it has the same nature for molecules of same kind, e.g. C – H bond length in alkanes. This term is described either as in the form of simple harmonic oscillator or Morse function.

The form of the bond stretching energy in the harmonic oscillator is described as:

$$E_B = \frac{1}{2} k_e (R - R_e)^2 \quad (14)$$

and in the Morse function as:

$$E_B = D_e (e^{-\alpha(R-R_e)} - 1)^2 \quad (15)$$

The value  $R_e$  does not signifies the equilibrium bond distance as it might seem apparently. It is the value of the bond length in a virtual unperturbed state. For unstrained molecules however this value is close to equilibrium value. The Morse function by Morse (1929) does a better job as it includes anharmonic terms near equilibrium and also it gives a finite value of energy when it comes to breaking bonds as oppose to harmonic oscillator function. However if the starting structure of the system is way off than the equilibrium one than from the energy derivative of Morse function the calculated restoring force will very less and hence harmonic function will do a better job in quickly bringing the structure to near equilibrium. The default form of bond stretching function in Dreiding is the harmonic form.

• **Angle bending:** For describing the relation between the energy of a system with the different angle bending of the same Dreiding uses two forms of equation. Harmonic cosine form and harmonic angle form (Fig. 5). The harmonic form for an angle between IJK atoms, J being the center atom is described as:

$$E_{IJK} = \frac{1}{2} C_{IJK} (\cos \theta_{IJK} - \cos \theta_J^0)^2 \quad (16)$$

where  $\theta$  is the angle concerned. The equilibrium angle  $\theta_J^0$  is believed to be independent of atom I and K and hence is only referred by J. The harmonic angle form is described by:

$$E_{IJK} = \frac{1}{2} K_{IJK} (\theta_{IJK} - \theta_J^0)^2 \quad (17)$$

The default used is the harmonic cosine form because the other one does not lead to zero slope as  $\theta$  approaches  $180^\circ$ . The force field file contains the values of the parameters of the equations which are used for MD.

• **Torsion:** The interaction energy of torsion between two bonds IJ and KL connected through JK is described in the form of:

$$E_{IJK} = \frac{1}{2} V_{JK} [1 - \cos(n_{JK}(\vartheta - \vartheta_{JK}^0))] \quad (18)$$

where  $\vartheta$  is the dihedral or torsional angle which is defined as the angle between IJK and JKL planes.  $n_{JK}$  is the periodicity (how it is defined) and  $V_{JK}$  is barrier to rotation. The parameters are taken independent of I and L. The torsional parameters are based on the type of hybridization and hence independent of the particular type of atoms involved. The force field file contains the values of these parameters based on the type of hybridization.

• **Inversion:** This term accounts for the easiness/difficulty of keeping all four atoms in the same plane when one single atom is bonded with the other three (Fig. 5). Both for planar molecules and non-planar molecules this term is important to account for. Denoting the angle between the JIL and KIL plane as  $\psi$  and  $n=2$  (for planar centers) or  $n=3$  (for tetrahedral centers) the energy due to inversion is expressed as

$$E_{inv}(\psi) = \frac{1}{2} K_{inv} \{1 - \cos[n(\psi - \psi_0)]\} \quad (19)$$

• **Nonbonded Interactions:** There are two expressions by which nonbonded van der Waals interactions are described. Lennard – Jones (LJ) 12 -6 forms and the exponential 6 form. The LJ form is described as:

$$E_{vdw}^{LJ} = AR^{-12} - BR^{-6} \quad (20)$$

and the exponential 6 form described as:

$$E_{vdw}^{X6} = Ae^{-CR} - BR^{-6} \quad (21)$$

As can be seen the difference between the two forms is nothing but the way of describing the repulsive part. For very low distance between two atoms the LJ potential gives a very big repulsive force and hence throws the atoms away. Though the LJ potential however requires only two parameters for the evaluation of the potential and faster to compute (find out the reason) the exponential 6 form gives a better agreement for short range interactions. The default form used in Dreiding is however LJ. The parameter values are calculated differently if the interaction concerned is between two different types of atoms. The way it is calculated can be based on arithmetic or geometric combination of the parameters of the pure system.

• **Electrostatic interactions:** The interaction energy due to electrostatic interactions is calculated by:

$$E_q = k \frac{q_i q_j}{r_{ij}} \quad (22)$$

where  $q_i$  and  $q_j$  are the charges on the atoms and  $r_{ij}$  is the distance between them.  $k$  is a constant which takes care of the dielectric constant and unit consideration. Interactions are not calculated for atoms bonded to each other (1, 2 interaction) and those involved in angle terms (1, 2, 3 interactions) as these are taken care by bond and angle stretching interactions.

• **Hydrogen Bonding:** The center of charges and van der Waals interaction must be in the center of the atom in order to take the position of the point charge on an atom and center of the atom to be the same. Satisfying this constraint it is difficult to parameterize a force field which correctly predicts the structure and the bond energy of H<sub>2</sub>O dimer, predicts the sublimation energy and the structure of ice and using van der Waals parameter correctly for non hydrogen bonded system. Dreiding uses a separate term to account for hydrogen bonding to describe interaction involving hydrogen atom with that of very



electronegative atoms (N, O, F) associated with hydrogen bond. In that case in addition to van der Waals forces and electrostatic interactions, a hydrogen bonding potential of the following form is included.

$$E_{hb} = D_{hb} \left[ 5 \left( \frac{R_{hb}}{R_{DA}} \right)^{12} - 6 \left( \frac{R_{hb}}{R_{DA}} \right)^{10} \right] \cos^4(\theta_{DHA}) \quad (23)$$

where  $\theta_{DHA}$  is the bond angle between hydrogen donor (D), hydrogen (H) and hydrogen acceptor (A).  $R_{DA}$  is the distance between donor and acceptor atoms and the values of  $D_{hb}$  and  $R_{hb}$  depends on the convention for assigning charges.

### 2.2.1.3.2 Morse Charge Equilibration (MS-Q) Force Field [25]

A Morse-charge equilibration force field (MS-Q FF) originally built up for bulk oxides  $Al_2O_3$  and  $SiO_2$ . MS-Q FF has been used for modeling clay minerals and their interactions with representative organic molecules.

The concept behind MS-Q is that for ionic or polar materials, electrostatics is the dominant force determining the structure and properties of the material. However, the charges responsible for the electrostatic effects depend upon the atomic configuration of the neighboring atoms [26]. The MS-Q FF allows the atomic charges to readjust as a function of the instantaneous geometry using the charge equilibration (QEq) procedure [22] of Rappé and Goddard. In addition, to electrostatic interactions, MS-Q uses a two body Morse function to describe nonelectrostatic terms [27].

$$E_{ij}^{Morse}(R_{ij}) = D_0 \left\{ \exp \left[ -\gamma \left( \frac{R_{ij}}{R_0} - 1 \right) \right] - 2 \exp \left[ -\frac{\gamma}{2} \left( \frac{R_{ij}}{R_0} - 1 \right) \right] \right\} \quad (24)$$

Thus potential energy that is the interaction between atom i and j is given by

$$U_{ij}(R_{ij}) = D_{0ij} \left[ \chi_{ij}^2 - 2\chi_{ij} \right] + q_i \frac{q_j}{R_{ij}} \quad (25)$$

$$\text{where } \chi_{ij} = \exp \left[ -\frac{\gamma_{ij}}{2} \left( \frac{R_{ij}}{R_0} - 1 \right) \right]$$

where  $D_{0ij}$  is the bond strength in kcal/mol,  $R_{0ij}$  is the bond distance in Å,  $\gamma_{ij}$  is a scale factor, and  $q_i$  is the partial charge if  $i^{\text{th}}$  atom [28].

Originally Morse-stretch potential charge equilibrium force field (MS-Q FF) has been developed to predict the phase changes in ionic insulators such as minerals and ceramics. The proposed MS-Q FF for silica system describes both four-fold and six-fold coordinated systems, silica glass and pressure-induced phase changes. It has been applied to various zeolites, silicates and alumina-silicates [28] and high pressure behavior of geophysical materials [29].

### 2.2.2 Ensembles

In mathematical physics, especially as introduced into statistical mechanics and thermodynamics by J. Willard Gibbs in 1878, an ensemble (also statistical ensemble or thermodynamic ensemble) is an idealization consisting of a large number of mental copies (possibly infinitely many) of a system, considered all at once, each of which represents a possible state that the real system might be in.

The ensemble formalizes the notion that a physicist can imagine repeating an experiment again and again under the same macroscopic conditions, but, unable to control the microscopic details, may expect to observe a range of different outcomes.

When an ensemble has an infinite number of members, it can be seen as defining a probability measure on the state space (phase space) of the system. Even though the dynamics of the real single system (for example, a complete gas of molecules, or a complete stock market) may be incalculably complex, or stochastic, or even discontinuous, the *average* (statistical) properties of the ensemble of possibilities as a whole may remain well defined, smoothly evolving, or for systems at macroscopic equilibrium even stationary. The notional size of the mental ensembles in thermodynamics, statistical mechanics and quantum statistical mechanics can be very large indeed, to include every possible microscopic state the system could be in, consistent with its observed macroscopic properties. But for important physical cases it can be possible, by clever mathematical manipulations, to calculate averages directly over the whole of the thermodynamic ensemble, to obtain explicit formulas for many of the thermodynamic quantities of interest, often in terms of the partition function  $Z$ , which encodes the underlying physical structure of the system [30].

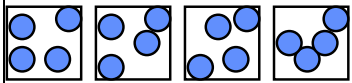
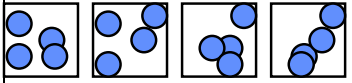
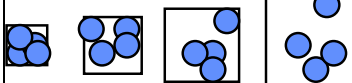
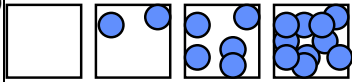
### 2.2.3 Types of Molecular Dynamics

There are three flavors of MD in common use and their acronyms are:

- ❑ NVE—indicates that during the dynamics the number of particles (N), volume (V), and energy (E) are kept constant. Since basic MD is simply to solve the Newton's equation of motion, the natural MD simulation is known to be microcanonical. This ensemble can be used to check the correctness of an algorithm. Also it can serve to test the adequacy of a time step by checking conservation of total energy [31].
- ❑ NVT—differs from standard Newtonian dynamics (NVE) in that the energy of the system is allowed to fluctuate as if the system were in thermodynamic equilibrium with a bath at fixed temperature (T) by using a thermostat. Several methods have been developed to serve the purpose; stochastic method, constraint methods (velocity-scaling and isokinetic method), and extended system method. The extended system method has been widely used because it produces a canonical distribution of microstates [13].
- ❑ NPT—differs from NVT dynamics in that the volume of the system is allowed to change in the same way as it would for a system in thermodynamic equilibrium with a pressure bath at fixed pressure (usually 1 atmosphere). It allows the system to adopt the density determined by the FF.
- ❑  $\mu$ VT—To consider theories for fluctuations in the number of particles we require an ensemble that keeps V, T, and the chemical potential,  $\mu$  constant, a grand canonical ensemble. To construct the grand canonical ensemble, the system is enclosed in a container that is permeable both to heat and to the passage of particles. The number of particles in the system can range over all possible values.

All types of ensembles' properties are shown in Table 2.

**Table 2.** Types of ensembles

Name	All states of	Probability distribution	Schematic
Microcanonical (NVE)	Given NVE	$\pi_i = \frac{1}{\Omega}$	
Canonical (NVT)	all energies	$\pi(E_i) = \frac{1}{Q} e^{-\beta E_i}$	
Isothermal-isobaric (NPT)	all energies and volumes	$\pi(E_i, V_i) = \frac{1}{\Delta} e^{-\beta(E_i + PV_i)}$	
Grand-canonical (μVT)	all energies and molecule numbers	$\pi(E_i, N_i) = \frac{1}{\Xi} e^{-\beta(E_i + \mu N_i)}$	
Ensemble	Thermodynamic Potential	Partition Function	Bridge Equation
Microcanonical	Entropy, S	$\Omega = \sum 1$	$S / k = \ln \Omega(E, V, N)$
Canonical	Helmholtz, A	$Q = \sum e^{-\beta E_i}$	$-\beta A = \ln Q(T, V, N)$
Isothermal-isobaric	Gibbs, G	$\Delta = \sum e^{-\beta(E_i + PV_i)}$	$-\beta G = \ln \Delta(T, P, N)$
Grand-canonical	-PV	$\Xi = \sum e^{-\beta(E_i + \mu N_i)}$	$\beta PV = \ln \Xi(T, V, \mu)$

## 2.3 Ab-Initio Calculations

Methods using the Hartree-Fock or DFT to calculate the electronic structure and associated properties are called ab-initio or first principles calculations, i.e. without the need for empirical fitting parameters. Ab-initio calculations are computationally costly. Though theories associated with ab-initio calculations were developed several decades ago, only in the last two decades ab-initio calculations have developed into one of the most important methods in atomistic modeling mostly due to more and more powerful computational resources become available.

The ab-initio methods are usually used to calculate the band structure, associated properties with the band structure, electronic and magnetic properties of systems, the phonon dispersion and thermal properties. Combined with MD, MC, transition state theory (TST), such as the nudged elastic band (NEB) method, ab-initio methods are also capable of simulating dynamic and kinetic problems.

### 2.3.1 Density Functional Theory

Density functional theory (DFT) is a formalism which allows the description of a system in terms of its electron density,  $\rho(\vec{r})$ . Based on the Hohenberg-Kohn theorem, the total electron energy can be written as a unique functional of the electron density,  $E[\rho(\vec{r})]$  [32]. The variational principle can be used to minimize the energy functional with respect to the density [33, 34],

$$\frac{\partial E[\rho(\vec{r})]}{\partial \rho(\vec{r})} = 0 \quad (26)$$

The total energy of an N-electron system contains the kinetic energy  $K[\rho(\vec{r})]$ , electron-nuclei interactions  $E_{el-nucl}[\rho(\vec{r})]$ , electron-electron interactions  $E_{el-el}[\rho(\vec{r})]$ , and the exchange-correlation energy  $E_{xc}[\rho(\vec{r})]$ ,

$$E[\rho(\vec{r})] = K[\rho(\vec{r})] + E_{el-nucl}[\rho(\vec{r})] + E_{el-el}[\rho(\vec{r})] + E_{xc}[\rho(\vec{r})] \quad (27)$$

$$\text{where, } E_{el-nucl}[\rho(\vec{r})] = \int V_{ext}\rho(r)d^3r \text{ and } E_{el-el}[\rho(\vec{r})] = \frac{1}{2} \iint \frac{\rho(r)\rho(\vec{r}')}{|\vec{r} - \vec{r}'|} d^3(\vec{r}) d^3(\vec{r}')$$

and  $V_{ext}$  is the external potential.

Since the functional dependence of the kinetic energy on the charge density is unknown, practical calculations need to use both the charge density and the wave functions, for which the kinetic energy can be easily calculated. Since the true many-electron wave function is computationally too demanding, the wave function is approximated by a linear combination of products of one-electron wave functions within an effective potential, consisting of the nuclei and the other electrons. Since such a one-electron approximation ignores the crucial electron-electron interactions, exchange and correlation, an approximation is needed to correct this error. The two most common approximations used today are called the local density approximation (LDA) and the generalized gradient approximation (GGA) [32].

LDA assumes that at each point  $\vec{r}$ , the exchange-correlation energy equals that of a system with constant  $\rho = \rho(\vec{r})$ . GGA, however, has an explicit dependence of the exchange-correlation functional on the gradient of the electron density. Both LDA and GGA are generally successful in a large variety of applications. However, LDA has a general tendency to overbinding. GGA has been shown to be quite successful in correcting some of the deficiencies of LDA. However, there are cases where the GGA may over-correct the deficiencies and lead to underbinding.

No matter if it is LDA or GGA, the total exchange-correlation energy of a system is the sum of the exchange-correlation energies per particle,  $\epsilon_{xc}[\rho(\vec{r})]$  (in the integral form):

$$E_{\text{xc}}\left[\rho\left(\vec{\mathbf{r}}\right)\right]=\int \epsilon_{\text{xc}}\left[\rho\left(\vec{\mathbf{r}}\right)\right]\rho\left(\vec{\mathbf{r}}\right)d^3\vec{\mathbf{r}} \quad (28)$$

Combining Eq. 26 to Eq. 28, variation of the total energy functional is

$$\frac{\partial E\left[\rho\left(\vec{\mathbf{r}}\right)\right]}{\partial \rho\left(\vec{\mathbf{r}}\right)}=\frac{\partial K\left[\rho\left(\vec{\mathbf{r}}\right)\right]}{\partial \rho\left(\vec{\mathbf{r}}\right)}+\int \frac{\rho\left(\vec{\mathbf{r}}\right)}{\left|\vec{\mathbf{r}}-\vec{\mathbf{r}}'\right|}d^3\vec{\mathbf{r}}'+V_{\text{ext}}\left(\vec{\mathbf{r}}\right)+\frac{\partial E_{\text{xc}}\left[\rho\left(\vec{\mathbf{r}}\right)\right]}{\partial \rho\left(\vec{\mathbf{r}}\right)} \quad (29)$$

where  $V_{\text{eff}}\left(\vec{\mathbf{r}}\right)=\int \frac{\rho\left(\vec{\mathbf{r}}\right)}{\left|\vec{\mathbf{r}}-\vec{\mathbf{r}}'\right|}d^3\vec{\mathbf{r}}'+V_{\text{ext}}\left(\vec{\mathbf{r}}\right)+\frac{\partial E_{\text{xc}}\left[\rho\left(\vec{\mathbf{r}}\right)\right]}{\partial \rho\left(\vec{\mathbf{r}}\right)}$  is defined as the effective

potential for the one-electron approximation. As mentioned earlier, the exact  $K[\rho(\vec{\mathbf{r}})]$  in

Eq. 29 is unknown. However, it can be calculated from the wave functions. To minimize

the energy in Eq. 29, we guess initial wave functions, calculate  $\rho(\vec{\mathbf{r}})$  from them and plug

them into the Schrödinger equation to obtain a new wave function set, electron density

and  $V_{\text{eff}}\left(\vec{\mathbf{r}}\right)$ , and then solve the Schrödinger equation again with the newly generated

$V_{\text{eff}}\left(\vec{\mathbf{r}}\right)$  and wave functions until it is converged. These are self-consistent cycles known

as the Kohn-Sham equations (Fig. 6).

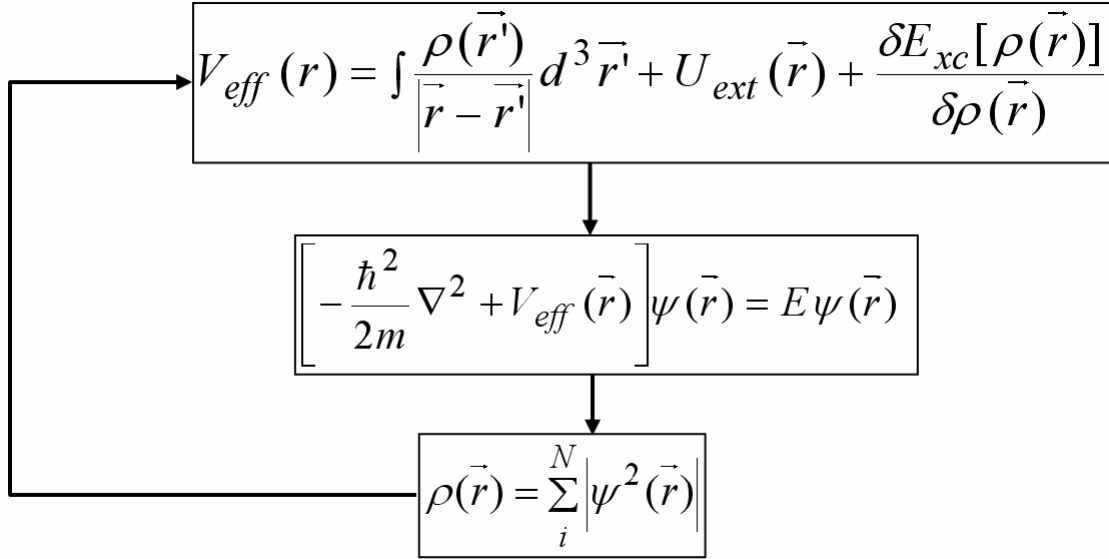


**Fig. 6.** Schematic illustration of the self-consistent cycles in ab initio calculations

In the Kohn-Sham equations, the wave functions are expanded into a basis for computational efficiency. The most common wave function basis for periodic systems consists of plane waves, a 3-D Fourier series

$$\psi_k(\vec{r}) = \sum_G a_{k+G} e^{i(k+G)\vec{r}} \quad (30)$$

where  $a_{k+G}$  is a constant,  $k$  is a wave vector in the Brillouin zone,  $G$  represents a lattice vector in reciprocal space.

However, calculations involving all electrons are still time-consuming. Since the valence electrons (electrons located in incompletely filled shells, e.g.  $3s^2$  and  $3p^2$  electrons for Si) dominate bonding, calculations are usually restricted to the valence electrons. All the effects of the core electrons (electrons in completely filled shell, such as  $1s^2$ ,  $2s^2$ , and  $2p^6$  electrons for Si) and nuclei are incorporated into an effective potential, a so-called pseudopotential [35]. The computers today are capable of conducting ab-initio calculations using pseudopotentials and a plane wave basis set on systems with 3000 atoms. The ab-initio calculations within this dissertation are primarily performed by using the Vienna Ab-initio Simulation Package (VASP) [36, 37]. VASP is a complex package for performing ab-initio quantum-mechanical calculations and molecular dynamic (MD) simulations using pseudopotentials and a plane wave basis set. Due to its completeness,



efficiency, and open-source distribution, it is probably the most widely used code of its kind today. The detailed algorithms and performance of VASP are well documented on its website [cms.mpi.univie.ac.at/vasp/vasp/vasp.html](http://cms.mpi.univie.ac.at/vasp/vasp/vasp.html). VASP calculations are known to obtain accurate bonding energies, structural configurations, system energies, phonon dispersions [38, 39], band structures (apart from the band gap, which is predicted smaller than experiments due to neglecting the true exchange effects), and density of states (DOS) of systems.

### 2.3.2 Advantages and Limitations of Ab-Initio Calculations

The ab-initio methods are based on solving the electronic Schrödinger equation. Compared with empirical pair potentials and semi-empirical methods, it has the following advantages:

- a) No experimental bias;
- b) Prediction of novel structures (no experimental data are required);
- c) Calculating more accurate data and
- d) Providing electronic states.

Ab-initio calculations are computationally expensive. Even today's fastest supercomputers can only conduct ab-initio calculation using pseudopotentials and a plane wave basis set on systems with no more than a few thousand atoms. More practically, the system is constrained to several hundred atoms. Obviously, it is thus impossible to use ab-initio calculations to exactly simulate a doped system with dopant concentrations less than 1/3000 [32]. A possible solution is extrapolating the data obtained from highly doped systems to the range one is interested in. Another problem associated with the size limit of ab-initio calculations is a much higher surface/bulk ratio than in real situations. Periodic boundary conditions (PBC) are often used to solve this problem. However, the artificially added PBC may be inconsistent with the periodicity of the real systems and lead to other problems, such as extra strain due to PBC. Moreover, due to length and time scale of ab-initio calculations and the present computer speed, ab-initio calculations are more limited than a method using the empirical pair potential to simulate dynamic and kinetic problems, such as the chemical reaction and the diffusion process. A number of approaches based on transition state theory (TST) [40], such as the nudged elastic band

(NEB) method[41, 42], have been developed to accelerate the process and make ab-initio calculations more applicable to the simulation of structural evolution.

## 2.4 Properties from Simulation

First-order properties such as internal pressure, internal energy, density are directly obtainable by ensemble/time averaging of the corresponding microscopic quantities. Second-order properties, i.e. thermodynamic and mechanical response functions such as specific heat capacity, isothermal compressibility factor, thermal expansion coefficient etc., may be obtained either using the finite difference approach or by using the appropriate statistical fluctuation formulae corresponding to these properties. To illustrate these two different approaches, consider four commonly used response functions in the isothermal isobaric ensemble (NPT): specific heat capacity at constant pressure ( $C_p$ ), isothermal compressibility factor ( $\kappa$ ), volumetric thermal expansion coefficient ( $\alpha$ ) and bulk modulus ( $\beta$ ). The finite difference method of estimation of these properties is based on their thermodynamic definitions shown in Eq. 31 – 34.

The specific heat capacity at constant pressure is the amount of system energy per unit mass required to raise the temperature by one degree Celsius at the same pressure. The relationship between energy and temperature change is usually expressed in the form shown below where  $C_p$  is the specific heat at constant pressure.

$$C_p = \left( \frac{\partial E}{\partial T} \right)_p \quad (31)$$

where  $E$  is the system energy.

Isothermal compressibility,  $\kappa$ , is the fractional change in volume of a system as the pressure changes at constant temperature. Isothermal compressibilities are derived from the slopes of P-V diagram by using Eq. 32.

$$\kappa = -\frac{1}{V} \left( \frac{\partial V}{\partial P} \right)_T \quad (32)$$

Thermal expansion coefficient is the fractional change in the volume of a system with temperature at constant pressure. Thermal expansion coefficient is derived from the slopes of V-T diagram by using Eq. 33. When volume expands sharply, this temperature is called melting temperature. Thermal expansion coefficients are usually positive

because increasing temperature causes a loosening up of the intermolecular bonds in the material.

$$\alpha = \frac{1}{V} \left( \frac{\partial V}{\partial T} \right)_P \quad (33)$$

Bulk modulus is defined by;

$$\beta = -V \left( \frac{\partial P}{\partial V} \right)_T = \rho \left( \frac{\partial P}{\partial \rho} \right)_T \quad (34)$$

where V stands for volume, P for pressure, T for temperature and  $\rho$  for density. Bulk modulus is related to the change in volume of the material when an external force is applied uniformly in all direction. If there is one directional compression or tensile strain occurs on one surface of a body, there some amount of strain is also developed in other directions.

The statistical fluctuation formulas for estimating these properties are given by [43]:

$$C_p = \frac{\langle E^2 \rangle - \langle E \rangle^2}{kT^2} \quad (35)$$

$$\kappa = \frac{\langle V^2 \rangle - \langle V \rangle^2}{\langle V \rangle kT^2} \quad (36)$$

$$\alpha = \frac{\langle VE \rangle - \langle V \rangle \langle E \rangle}{\langle V \rangle kT^2} \quad (37)$$

$$\beta = \frac{NkT}{V} + V \left\langle \frac{\partial^2 U}{\partial V^2} \right\rangle - \frac{V \delta \left[ \frac{\partial U}{\partial V} \right]^2}{kT} \quad (38)$$

where the angular brackets represent a time average of the corresponding system property. Eq. 30 – 33 are rigorously valid in the thermodynamic limit of an infinite size system. Derivations for the finite  $N$  case have been made and the exact and thermodynamic limit formulae were compared to Eq. 35 – 38 [44]; differences were found to be less significant than the other systematic and random errors for systems of size  $N$  as low as 200–300 particles [43].

We aim at predicting properties of the materials are targeted via molecular simulations. These include anisotropic mechanical properties such as elastic constants [24, 45]. A Taylor expansion of the energy of a unit cell around the minimum energy structure can be expressed as;

$$E(\boldsymbol{\varepsilon}) = E_0 + \sum_i^6 \left. \frac{\partial E}{\partial \varepsilon_i} \right|_0 \varepsilon_i + \frac{1}{2} \sum_{i,j}^6 \left. \frac{\partial^2 E}{\partial \varepsilon_i \partial \varepsilon_j} \right|_0 \varepsilon_i \varepsilon_j + \dots \quad (39)$$

where  $E_0$  refers to energy in the equilibrium configuration. The third term on the RHS of the equation are the second derivative of energy with respect to strains, hence related to second order elastic constants of the material. In its most general form, a material can have 21 independent elastic constants (due to commutativity in the second derivative, resulting 6x6 matrix is symmetric). For higher symmetries, such as in cubic crystals one has only 3 independent (9 non-zero elastic constants).

In order to calculate the mechanical properties of the pure MMT system concerned, the method in [24] was applied. To calculate the elements  $C_{ij}$  of the stiffness matrix strain  $\varepsilon_{ij}$  was applied to the system in a systematic form and molecular simulation was done in NVT ensemble and the stress  $\sigma_{ij}$  was calculated in Eq 40. Both tensile and compressive strains are applied. The elastic constant or in other words stiffness constant is calculated as;

$$C_{ij} = \frac{(\sigma_{i+} - \sigma_{i-})}{(\varepsilon_{j+} - \varepsilon_{j-})} \quad (40)$$

Elements of stiffness matrix then may be calculated by calculating the elements of above equation for  $j = 1$  to 6.

For elastic deformation, the constant of proportionality between stress and strain is called Young's modulus or elastic modulus, given by Eq 41.

$$E_{ij} = \frac{\sigma_{ij}}{\epsilon_{ij}} \quad (41)$$

where  $\sigma_{ij}$  is tensile stress and  $\epsilon_{ij}$  is tensile strain.

Poisson's ratio,  $\nu$ , is the ratio of transverse contraction strain,  $\epsilon_{yy}$ , to longitudinal extension strain,  $\epsilon_{xx}$ , in the direction of stretching force (Eq. 42). Tensile deformation is considered positive and compressive deformation is considered negative. The definition of Poisson's ratio contains a minus sign so that normal materials have a positive ratio.

$$\nu = -\frac{\text{transverse strain}}{\text{longitudinal strain}} = -\frac{\epsilon_{yy}}{\epsilon_{xx}} \quad (42)$$

Lame's constants are derived from modulus of elasticity and Poisson's ratio, given by Eq. 43 - 44.

$$\lambda = \frac{\nu E}{(1 + \nu)(1 - 2\nu)} \quad (43)$$

$$\mu = \frac{E}{2(1 + \nu)} \quad (44)$$

## 2.5 A Survey of Earlier Work on Clay-Polymer Composites Literature Survey

Pospíšil et. al. used molecular mechanics and molecular dynamics simulations combined with X-ray powder diffraction to investigate the structure and energy characteristics of Na<sup>+</sup> montmorillonite intercalated with neutral molecules of ODAMIN. The exfoliation is easier for the bilayer arrangement of the guests and that the exfoliation energy decreases with the increase in ODAMIN concentration. The main aim of their study was to prepare intercalate that will be useful as a precursor for subsequent intercalation of further polar organic molecules and intercalate with a low energy of exfoliation for potential use in polymer/clay nanocomposites technology.

Pruissen and coworkers analyzed the charge distribution in di- and trioctahedral smectites intercalated with the Keggin cation:  $[\text{Al}_{13}\text{O}_4(\text{OH})_{24}(\text{H}_2\text{O})_{12}]^{7+}$  (further denoted as  $[\text{Al}_{13}]^{7+}$ ). The structure of this cation is the fragment of a salt structure with rigidly bound hydroxyl groups and water molecules. The oxygens belonging to the hydroxyl groups and the water molecules are all bonded to the Al atoms in the Keggin ion ( $\text{AlO}_6$  octahedra). This Keggin ion can be ion exchanged on smectite clays with the preservation of its structure.

Klika and coworkers focused on montmorillonite (host) intercalation by rhodamine B (guest). This dye is utilized as a laser pigment, as a sensitizer in various photochemical reactions, or as a source for singlet oxygen formation [46]. In water solutions, rhodamine B aggregates, forming dimers. The proportion of the dimers to the monomers increases with increasing concentration of dye. Except for interaction strengths between dye monomers, the formation of dimers is also influenced by the surrounding environment properties, e.g., dye concentration, pH, and ionic strength. The intercalation of dye (guest) into montmorillonite (host) runs on the principle of the ion-exchange reaction. This process was controlled by Coulombic and van der Waals strengths, H-bonds, and also nonbond energy contributions between guest and host and between guest and guest [46].

Zeng and coworker investigated organic-inorganics nanocomposites. Molecular dynamics (MD) simulation is used to probe the layering behavior and interlayer structure

of quaternary alkylammonium modified montmorillonites at a molecular level. They chose specifically the quaternary alkylammoniums as the guests because there is a wealth of experimental XRD data on these organoclays and they are widely used as precursors in the preparation of polymer nanocomposites [47]. Comparison will be made between the simulated and experimental results mainly in terms of the basal spacings. These results will be used to examine the validity of our MD approach to the organoclay systems. The atomic density profiles and arrangement of alkyl chains will also be produced and discussed [47].

## CHAPTER III

### RESULTS AND DISCUSSIONS

#### 3.1 Computational Details

In other words to produce nanocomposite material depending on knowledge of structure-property relationship with preferred material strength, mechanical and other properties tailored to application requires and economically allowable. We conducted our computational experiments using molecular dynamics methods with reliable force fields for Na-MMT, molecular mechanics and ab-initio DFT calculations. We employed crystal builder utilities, molecular mechanics and molecular dynamics utilities of the software package of Cerius<sup>2</sup> (Accelrys, San Diego, CA, USA) with force fields for clays [Demiralp, Cagin, Goddard]. These computations are performed on SGI Octane2 systems in Cagin Computer Laboratory. Ab-initio calculations are performed with Vienna Ab-initio Simulation Package (VASP). These DFT calculations are done by using Apple 2.3 GHz Xserve G5 cluster (CAT) of the Department of Chemical Engineering or SGI Altix 3700 (COSMOS) at Texas A&M University Supercomputing Facility using multiple cpus, typically 8 to 16 cpus.

##### 3.1.1 Interaction Force Field: Functional Forms and Parameters Used in Simulations

General force constants and geometry parameters for the Dreiding force field are based on simple hybridization rules rather than on specific combinations of atoms. The Dreiding force field does not generate parameters automatically. The Dreiding force field has good coverage for organic, biological and main-group inorganic molecules. It is only moderately accurate for geometries, conformational energies, intermolecular binding energies, and crystal packing.

The van der Waals interactions are described by the Lennard–Jones potential. Electrostatic interactions are described by atomic monopoles and a screened Coulombic term. Hydrogen bonding is described by an explicit Lennard–Jones 12–10 potential [21].



$$E_{hb} = D_{hb} \left[ 5 \left( \frac{R_{hb}}{R_{DA}} \right)^{12} - 6 \left( \frac{R_{hb}}{R_{DA}} \right)^{10} \right] \cos^4(\theta_{DHA})$$

$$E_{\text{Bond}} = \frac{1}{2} k_e (R - R_e)^2$$

$$E_{\text{angle}} = \frac{1}{2} k_{ijk} (\theta_{ijk} - \theta_j^o)^2$$

$$E_{\text{coul}} = \sum_{i,j} 322.06 \frac{q_i q_j}{\epsilon r_{ij}}$$

### *Morse Charge Equilibration (MS-Q) Force Field [25]*

We choose the MS-Q force field (FF) developed by Demiralp et al for the bulk oxides SiO<sub>2</sub> and Al<sub>2</sub>O<sub>3</sub> [25] to model clay minerals for the study of the interactions with inorganic molecules. A unique aspect of the MS-Q FF is that the atomic charges are allowed to change self-consistently during the simulation. The MS-Q FF reproduces the structural parameters for these minerals and gives accurate enthalpies of immersions in water, organic solvents and hydrocarbons. Some parameters have shown in Table 3 and Table 4. Whole MSQ-Clay FF parameteres have shown in APPENDIX B.

**Table 3.** Diagonal Morse type van der Waals potential

Atom types	Atom names	Mass (g/mol)	R <sub>o</sub> (Å)	D <sub>o</sub> (kcal/mol)	γ
H_C	Hydrogen	1.000800	3.3472	0.3796x10 <sup>-4</sup>	12.0000
O_3C	Oxygen(hydrogen bonding donor)	15.99940	3.7835	0.5363	10.4112
O_AC	Oxygen(hydrogen bonding acceptor)	15.99940	3.7835	0.5363	10.4112
Al3C	Aluminum	26.98150	3.8915	0.3321	11.9071
Si3C	Silicon	28.08600	3.4103	0.2956	11.7139

**Table 4.** Off-diagonal Morse type van der Waals potential

Atom types	$R_o$ (Å)	$D_o$ (kcal/mol)	$\gamma$
O_AC ... O_3C	3.7835	0.5363	10.4112
Al3C ... O_3C	1.7775	26.03	9.7830
Al3C ... O_AC	1.7775	26.03	9.7830
Si3C ... O_3C	1.6248	46.00	8.3022
Si3C ... O_AC	1.6248	46.00	8.3022
O_3C ... H_C	1.0770	19.55	8.4394
O_AC ... H_C	2.1768	0.1753	16.0000
Si3C ... Al3C	4.0949	0.0000	8.7732

### 3.1.2 Model Construction and Molecular Dynamics of MMT

The chemical structure of MMT is built from a 2:1 layered mineral pyrophyllite structure. MMT is an aluminosilicate made up of a central aluminate octahedral sheet sandwiched between two silicate tetrahedral sheets. Chemical structure is built by using crystallographic atomic coordinates [48, 49] which are shown in Table 6. In our research, we built the crystal of  $\text{Na}^+$ -MMT using the Crystal Builder of Cerius<sup>2</sup> (Accelrys, San Diego, CA, USA). The lattice structure is monoclinic with space group C2/m. It is characterized by lattice parameters shown in Table 5 [49].  $\xi$ ,  $\eta$ ,  $\zeta$  atomic coordinates calculation is explained in APPENDIX A. The model system for molecular mechanics and dynamics system was chosen as a 3x2x2 super lattice of the unit cell.

**Table 5.** Lattice parameters of Na-montmorillonite [49]

a	5.20 Å	$\alpha$	90°
b	9.20 Å	$\beta$	99°
c	10.13 Å	$\gamma$	90°

We particularly modeled the bulk, surface and layer structure, energetics and thermodynamics using variable charge model force fields (MSQ-Clay force field developed by Demiralp et al.). The calculations to obtain the optimum structures have used the Minimizer module in Cerius<sup>2</sup>. An energy calculation is essentially just a zero-iteration minimization. Minimization is used to calculate the energy of the current model structure without changing any atom positions. In dealing with macromolecular optimization calculations, it is important to keep in mind the theoretical significance of the minimum- energy structure and its calculated energy. The calculated energy of a fully minimized structure gives the classical enthalpy at absolute zero.

While minimization computes the forces on the atoms and changes their positions to minimize the interaction energies, dynamics computes forces and moves atoms in response to the forces. Molecular dynamics solves the classical equations of motion for a system of  $N$  atoms interacting according to a potential energy force field as described in Section 2.2.1. Dynamics simulations are useful in studies of the time evolution of a variety of systems at nonzero temperatures.

NPT dynamics is used to determine bulk properties at constant atmospheric pressure and temperature is varied between 100 K and 600 K using the Nosé-Hoover thermostat. We used the results of the NPT simulations in isothermal–isochoric (NVT) molecular dynamics experiments to determine layering enthalpy also between 100 K and 600 K. Because large time step causes instability and inaccuracy in the integration process, whereas too small time step does not cause any harm, except for the waste of computer time, integration time step for MMT system is chosen 0.002ps. All simulations used same integration time step, and the length of the simulation was adjusted to ensure equilibration and proper sampling. In MD, relaxation time was taken 0.05ps and this procedure led to 25 ps for montmorillonite (12500steps).

**Table 6.** Na<sup>+</sup>-montmorillonite atomic coordinates [48, 49]

Atom	Fractional coordinates		
	$\xi$	$\eta$	$\zeta$
Al	0.000	0.333	0.000
Na	0.500	0.000	0.500
Mg	0.000	0.000	0.000
O1	0.481	0.500	0.320
O2	0.172	0.728	0.335
O3	0.348	0.691	0.110
OH	0.419	0.000	0.105
H	0.320	0.000	0.170
Si	0.417	0.329	0.270

In our research, bulk structure was two layered structure and for exfoliation kinetics MMT-alkyl amine structure and different layered structures as 1, 2, 4, 6, 8 and 12 layers are built in Cerius<sup>2</sup> shown in Fig. 7, Fig. 8, Fig. 9. After calculating energy change value for bulk structure, we compared energy changes for different layered structures with bulk structure and we calculated required energy values for breaking off layers from the Na-MMT structure as a function of one layer at room temperature and also calculated thermodynamic properties such as specific heat and thermal expansion coefficient.

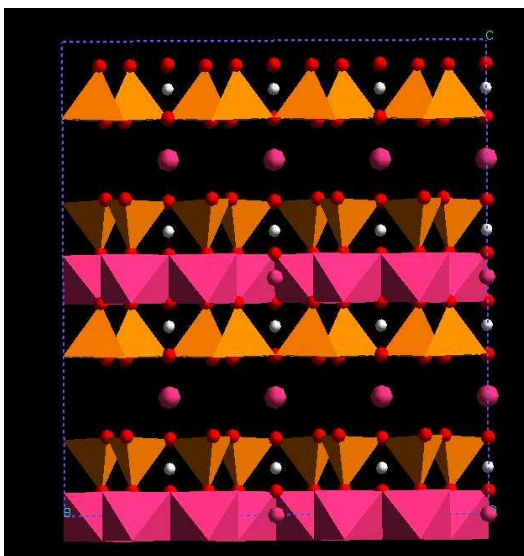


**Fig. 7.** Na<sup>+</sup>-MMT bulk structure

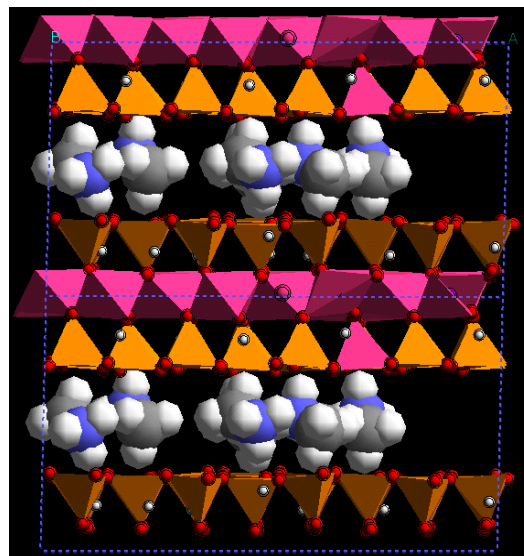


**Fig. 8.** MMT-NH<sub>3</sub>CH<sub>3</sub>

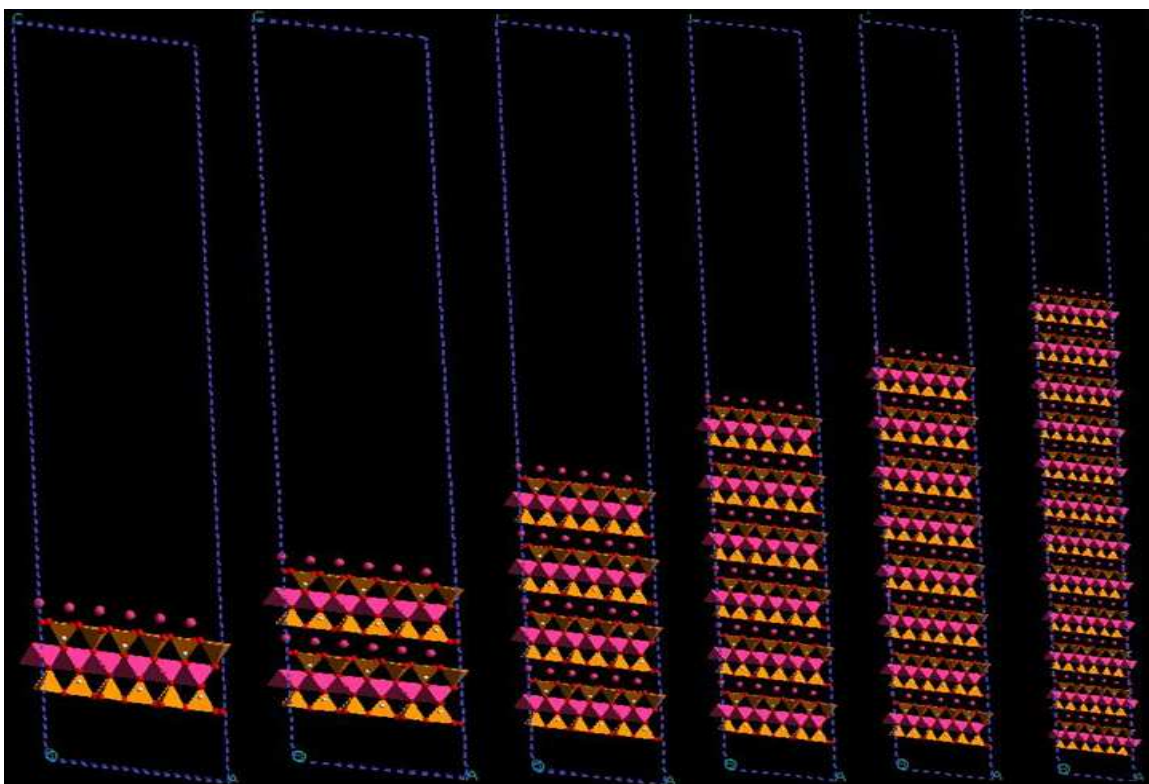


**Fig. 9.** Models of layered structures of Na<sup>+</sup>-MMT

### 3.2 Na<sup>+</sup>-MMT Bulk Structure (3x2x2) by Using NPT Molecular Dynamics

In this part, thermodynamic properties of Na<sup>+</sup>-MMT bulk structure have been calculated by using MD method. We used NPT ensemble for bulk structure. For various temperature and pressure, we determined specific heat capacities at constant pressure by using the total energy changes with respect to temperature (Fig. 10) and calculated specific heat capacity from Fig. 10 is shown in Table 7. On the other hand, increasing of total energy and enthalpy with increasing pressure is shown in Fig. 10 and Fig. 11.

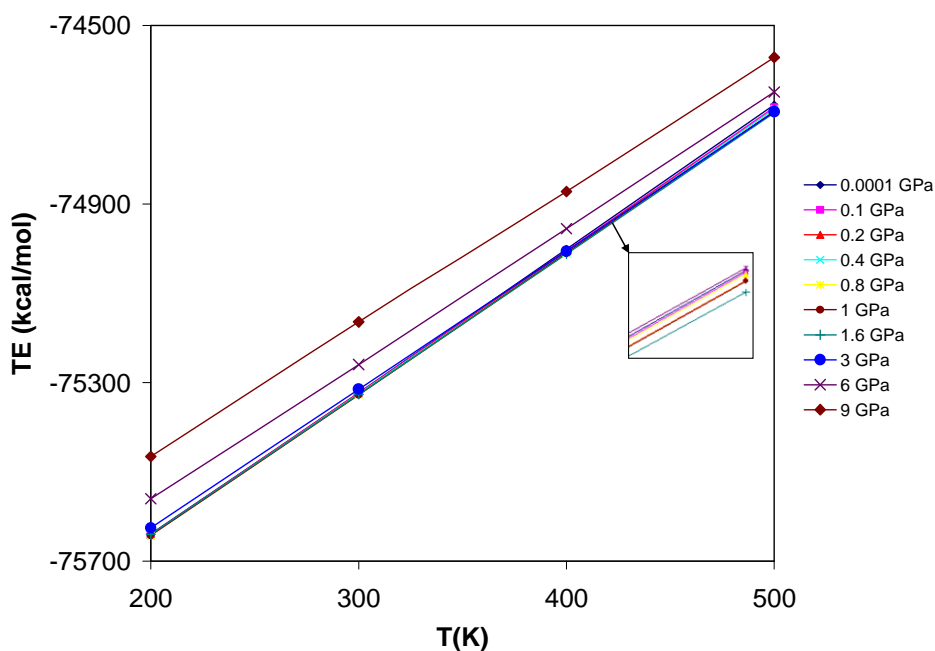


**Fig. 10.** Total energy changes with respect to temperature for Na<sup>+</sup>-MMT bulk structure (3x2x2) by using NPT molecular dynamics

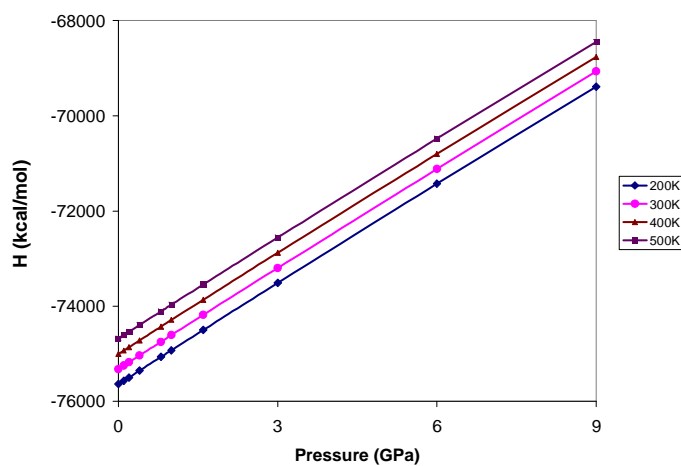


**Fig. 11.** Enthalpy changes with respect to pressure for Na<sup>+</sup>-MMT bulk structure (3x2x2) by using NPT molecular dynamics

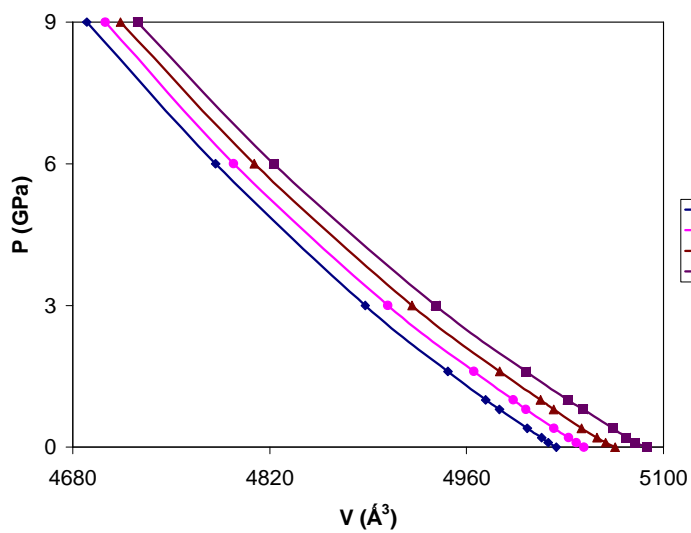


**Fig. 12.** Pressure changes with respect to volume for Na<sup>+</sup>-MMT bulk structure (3x2x2) by using NPT molecular dynamics (compressibility calculation)

Volume of bulk structure changes with applied pressure are shown in Fig. 12. Pressure and volume changes with respect to temperature are also figured out in Fig. 12. From this figure, we can easily calculate isothermal compressibility factor by using Eq. 31. Calculated isothermal compressibility factor is shown in Table 7 and temperature effect is plotted in Fig. 13. We have also looked at volume and lattice parameter changes with respect to temperature. After plotting Fig. 14 and Fig. 15, we calculated thermal expansion coefficient and linear thermal expansion coefficient by using their slopes.

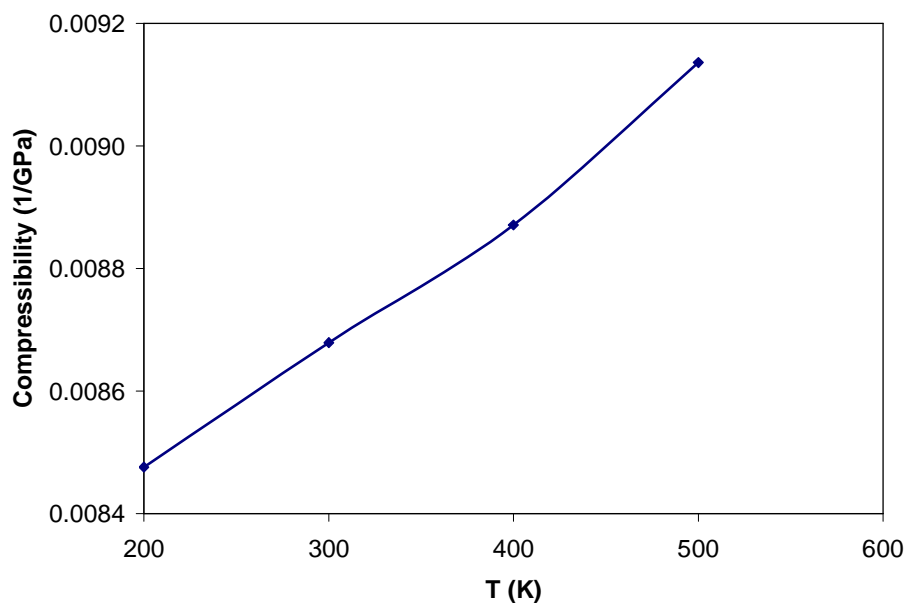


**Fig. 13.** Compressibility changes with respect to temperature for Na<sup>+</sup>-MMT bulk structure (3x2x2) by using NPT molecular dynamics



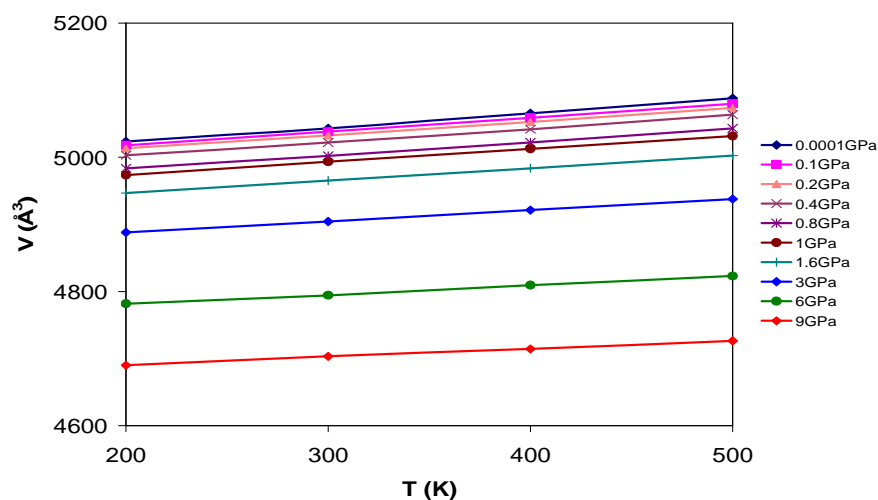


**Fig. 14.** Volume changes with respect to temperature for  $\text{Na}^+$ -MMT bulk structure ( $3 \times 2 \times 2$ ) by using NPT molecular dynamics (thermal expansion coefficient calculation)

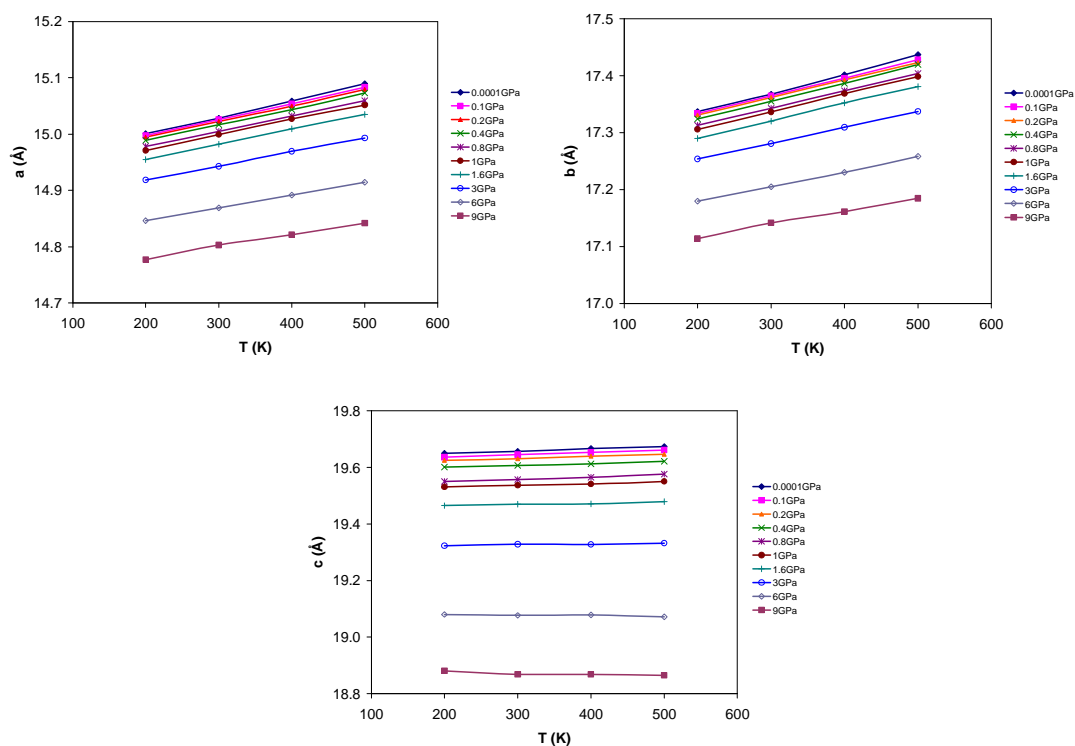


**Fig. 15.** Cell parameters changes with respect to temperature for  $\text{Na}^+$ -MMT bulk structure ( $3 \times 2 \times 2$ ) by using NPT molecular dynamics (linear thermal expansion coefficient calculation)

**Table 7.** Thermodynamic properties of Na<sup>+</sup>-MMT

	<b>Bulk (3x2x2)</b>	<b>Different Layered structure</b>	<b>Unit cell (1x1x1)</b>
<b>C<sub>p</sub> (kcal/molK)</b>	3.18	2.82	NA
<b>α (1/K)</b>	3.7*10 <sup>-5</sup>	3.8*10 <sup>-5</sup>	NA
<b>α<sub>linear</sub>(1/K)</b>	0.00002	NA	NA
<b>κ (1/GPa)</b>	0.0086	NA	0.0086

where

$$C_p = \left( \frac{\partial E}{\partial T} \right)_p \quad \alpha_{\text{linear}} = \frac{1}{a} \left( \frac{\partial a}{\partial T} \right)_p$$

$$\alpha = \frac{1}{V_o} \left( \frac{\partial V}{\partial T} \right)_p \quad \kappa = -\frac{1}{V_o} \left( \frac{\partial V}{\partial P} \right)_T$$

### 3.3 Different Layered Na<sup>+</sup>-MMT Structures

We have calculated required energies for peeling off layers from different layered structures at different temperatures between 200 and 500K. Break off energy was determined by converting all total energies of layered structures to 2 layered Na<sup>+</sup>-MMT total energies by using formula

$$\left[ \frac{\Delta E_{n \text{ layered structure}} * 2}{n} \right] \quad (45)$$

where n is number of layer because of comparing with our bulk structure. After that, we compared bulk and converted structures' energies and then calculated required energies for each layered structures and each temperatures. These relationships are shown in Fig. 16. On the other hand, we obtained that thin layered structure needs more energy than thick layered structure. Required energy for exfoliation becomes harder when temperature decreases because entropic contribution of the system increases. In Fig. 16, 8 layered structure has the maximum number of layer for exfoliation at low temperatures and 4 layered structure has the maximum number of layer for exfoliation at high temperatures.

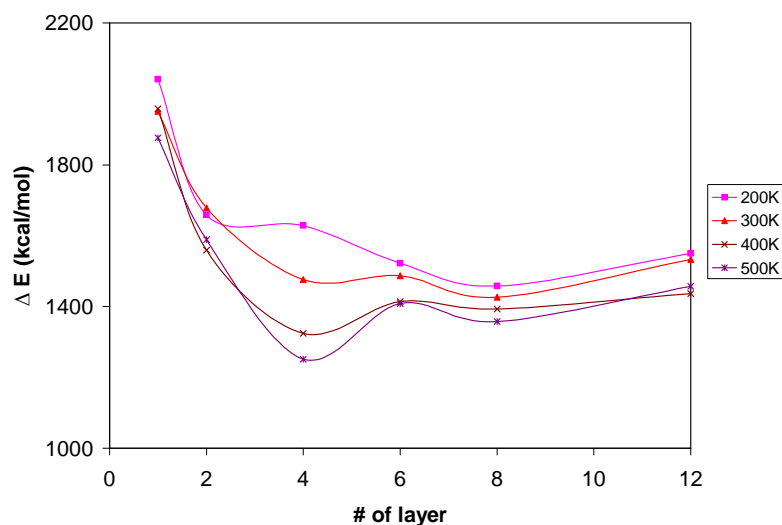


**Fig. 16.** Calculated required energy values for breaking off layers from the Na<sup>+</sup>-MMT structure as a function of one layer at different temperature

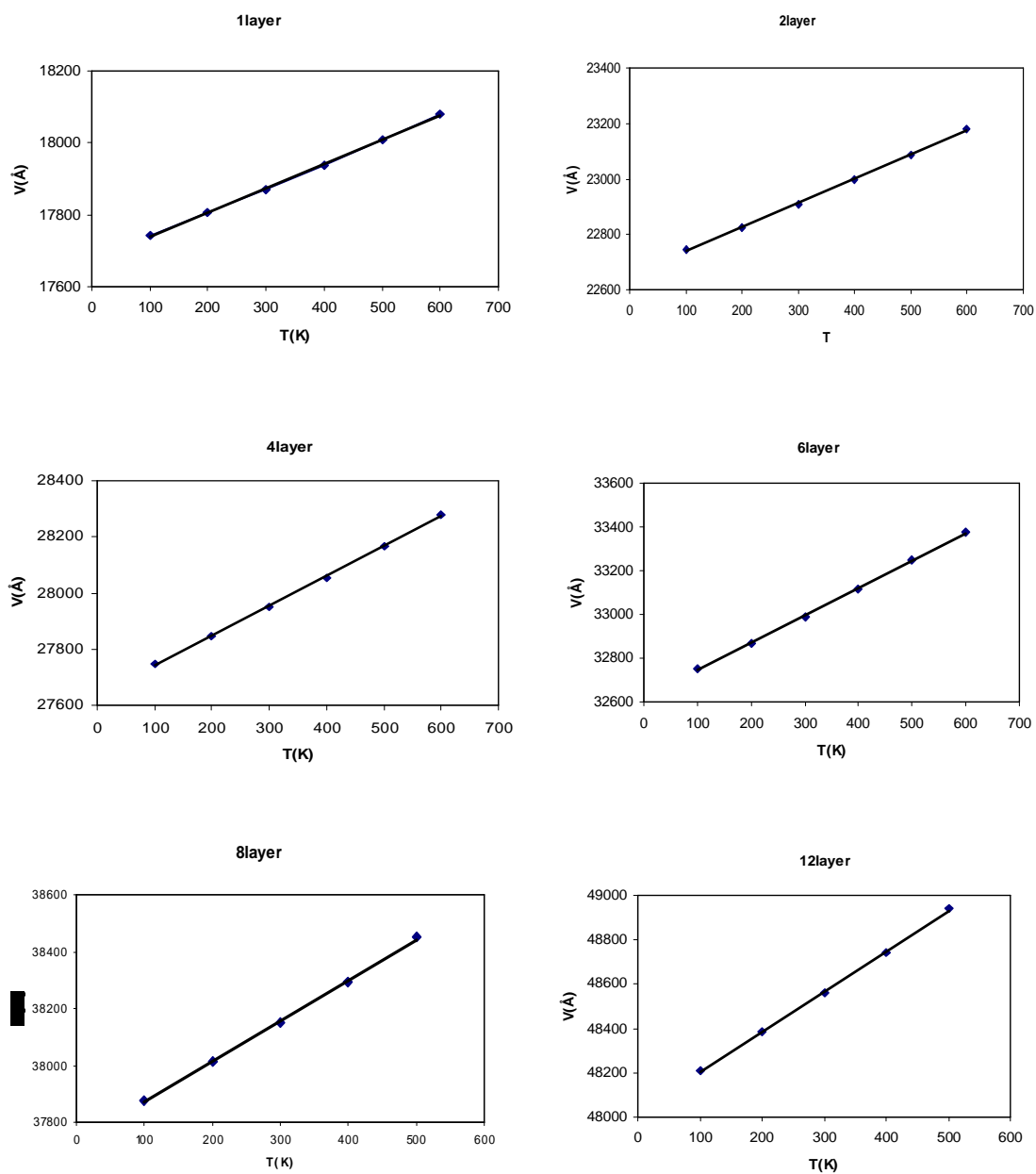


**Fig. 17.** Volume change with respect to temperature for different layered Na<sup>+</sup>-MMT structure (thermal expansion coefficient)

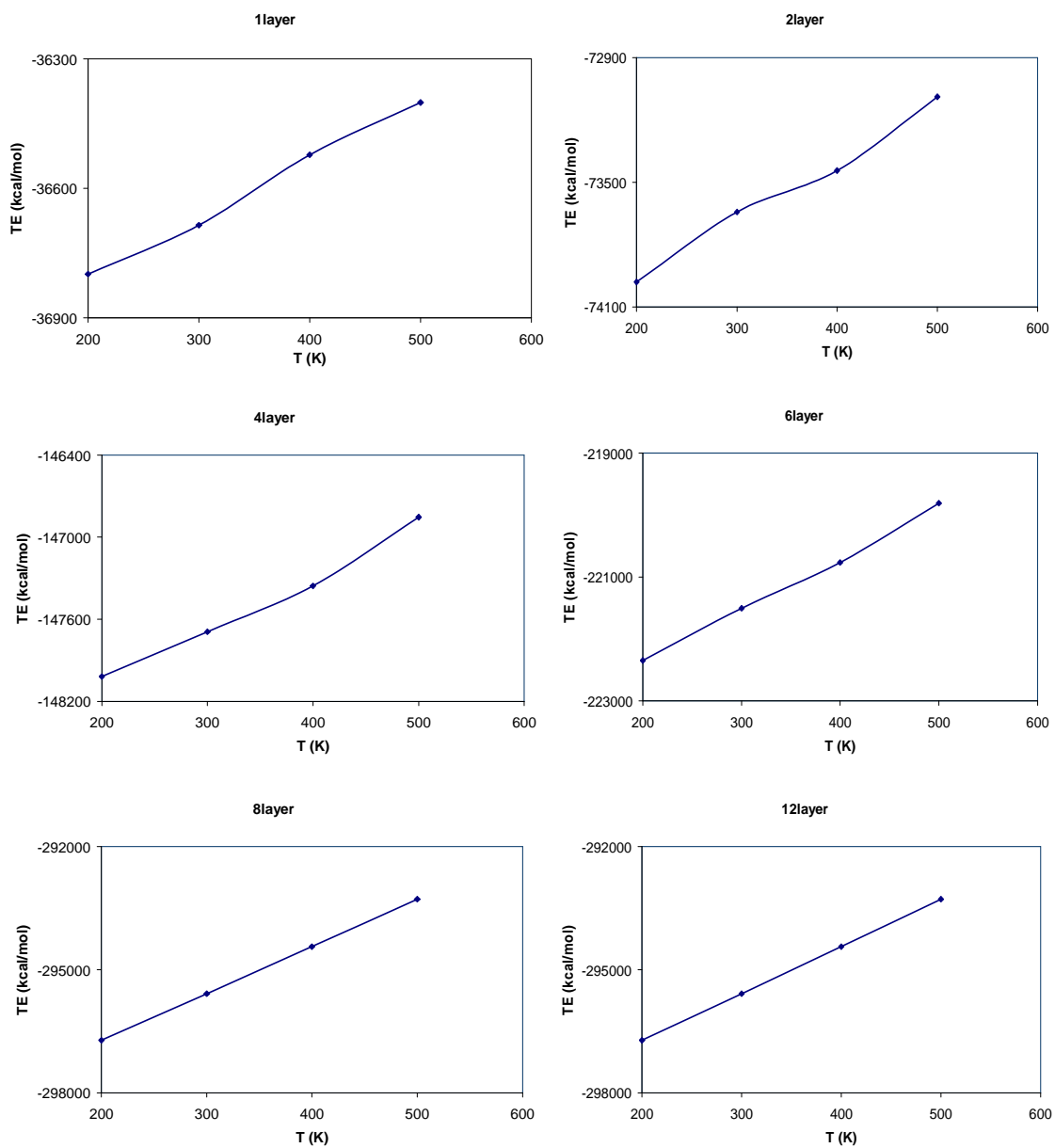


**Fig. 18.** Total energy changes with respect to temperature for different layered Na<sup>+</sup>-MMT structure (Cp calculation)

In Fig. 17, we analyzed that when system temperature increases, thermal expansion occurs for each different layered structure. When compared the results with bulk structure (Fig. 14), our results are comparable with layered structures shown Table 7 and also they are very similar with experimental result which is equal to  $3.6 \times 10^{-5} \text{K}^{-1}$  calculated by Yang et al [50].

In Fig. 18, we calculated specific heat capacity equal to 2.82 kcal/molK for layered structure at constant pressure by using finite difference method (Eq. 31).

### 3.4 $\text{Na}^+$ -MMT Unit Cell (1x1x1) by Using NVT Molecular Dynamics

Since the experimental elastic constant calculation is extremely difficult to obtain for clay structures, we aimed to fill this lack of knowledge by using simulation methods. In Fig. 19, Fig. 20, Fig. 21, Fig. 22 and Fig. 23, we tried to validate bulk moduli, stiffness constants, Young's moduli and lame constants, which are related with pressure changes. Results are taken directly from  $\text{Na}^+$ -MMT unit cell NVT calculations by using Cerius<sup>2</sup>.

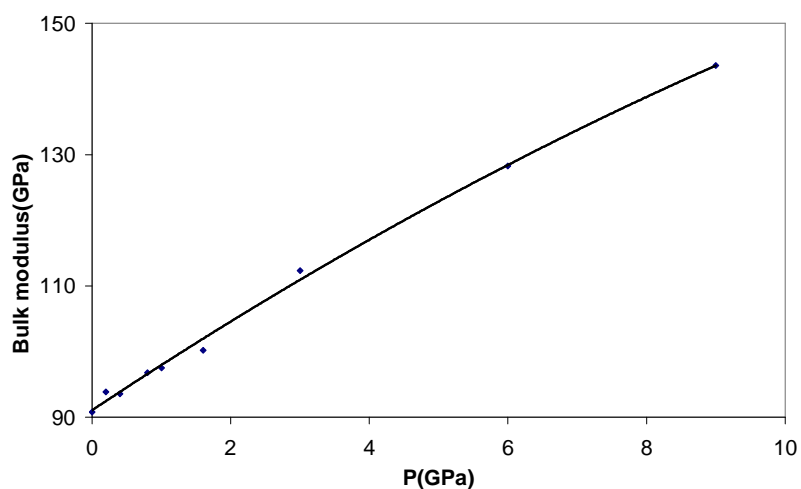


**Fig. 19.** Bulk modulus changes with respect to pressure for  $\text{Na}^+$ -MMT unit cell (1x1x1) by using NVT molecular dynamics at 300K

Young modulus in y direction is given as 178GPa in reference [51]. We calculated young modulus in y direction equal to 170.6GPa which is comparable with reference [51]. In Fig. 21 and Table 8, we showed Young's moduli changes for MMT with respect to various pressures.

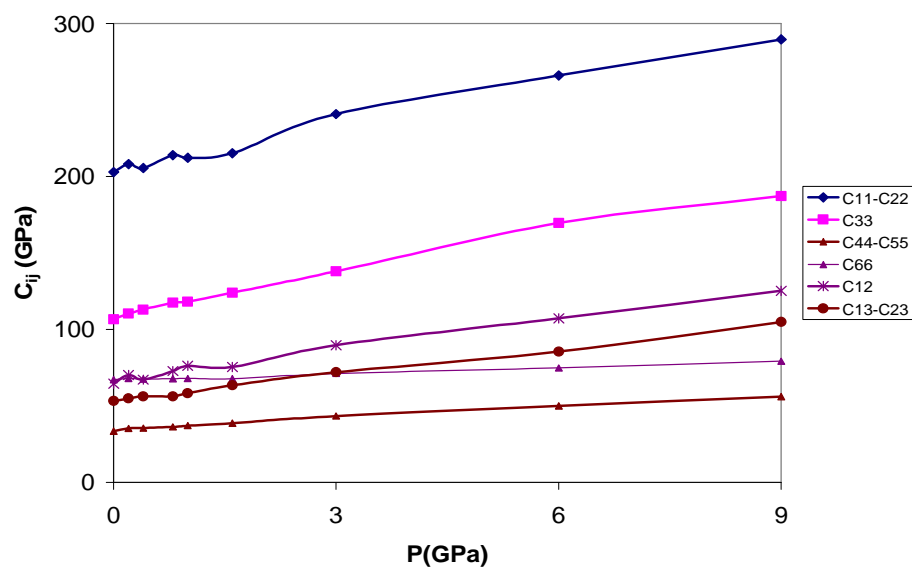


**Fig. 20.** Elastic constants changes with respect to pressure for  $\text{Na}^+$ -MMT unit cell ( $1 \times 1 \times 1$ ) by using NVT molecular dynamics at 300K

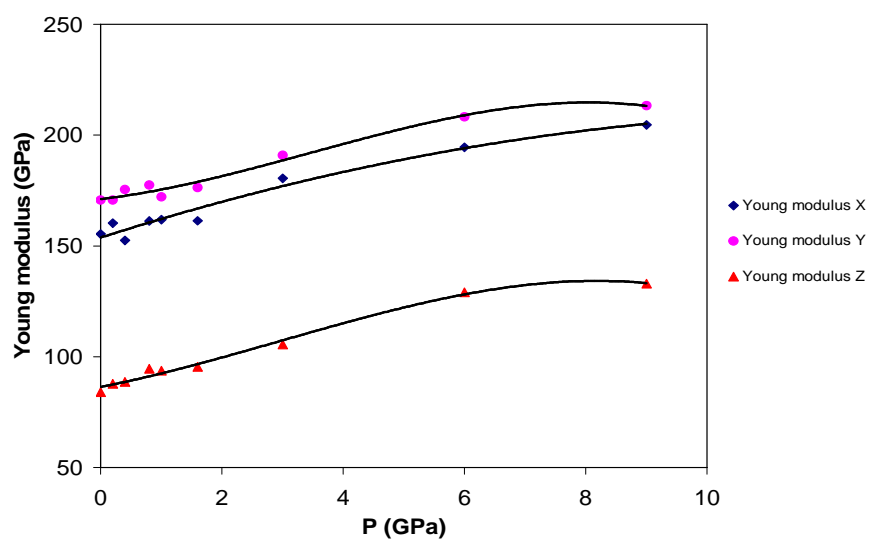


**Fig. 21.** Young's moduli changes with respect to pressure for  $\text{Na}^+$ -MMT unit cell (1x1x1) by using NVT molecular dynamics at 300K

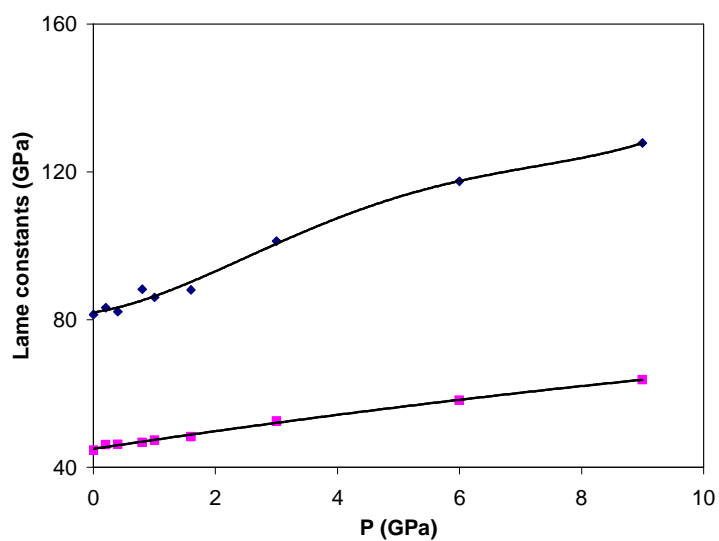


**Fig. 22.** Lamé constants changes with respect to pressure for  $\text{Na}^+$ -MMT unit cell (1x1x1) by using NVT molecular dynamics at 300K



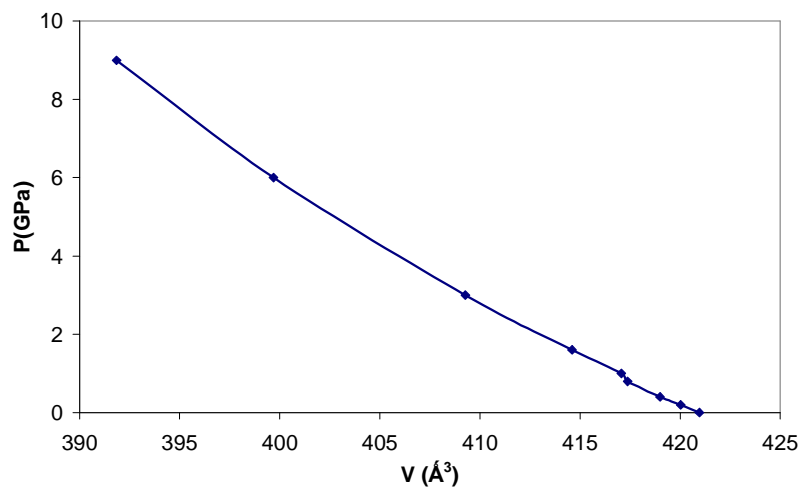


**Fig. 23.** Pressure changes with respect to volume for  $\text{Na}^+$ -MMT unit cell (1x1x1) by using NVT molecular dynamics at 300K

**Table 8.** Mechanical properties calculated by using Cerius<sup>2</sup> of Na<sup>+</sup>-MMT unit cell (1x1x1) at 300K

P(GPa)	Compressibility	Young Modulus			Poisson Ratios					
		X	Y	Z	E <sub>xy</sub>	E <sub>yx</sub>	E <sub>zx</sub>	E <sub>xz</sub>	E <sub>yz</sub>	E <sub>zy</sub>
0.0001	0.0118	155.3149	170.6272	84.0388	0.2028	0.2228	0.2245	0.4148	0.3833	0.1888
0.2	0.0114	160.26	170.7105	87.6926	0.2293	0.2442	0.2176	0.3976	0.368	0.189
0.4	0.0113	152.4851	175.4369	88.6011	0.1994	0.2294	0.2339	0.4026	0.3854	0.1947
0.8	0.0110	161.1767	177.4608	94.5516	0.2246	0.2472	0.2146	0.3657	0.3644	0.1941
1	0.0107	161.9162	172.0571	93.6224	0.2493	0.2649	0.2192	0.3791	0.3598	0.1958
1.6	0.0102	161.3066	176.2275	95.389	0.2231	0.2437	0.2377	0.402	0.3875	0.2097
3	0.0091	180.5427	190.956	105.6186	0.2449	0.259	0.2324	0.3973	0.3868	0.2139
6	0.0076	194.4966	208.311	129.0092	0.2717	0.291	0.2473	0.3728	0.3579	0.2217
9	0.0067	204.6693	213.272	133.0092	0.275	0.2866	0.2538	0.3906	0.4174	0.2603

**Table 9.** Mechanical properties calculated by using Cerius<sup>2</sup> of Na<sup>+</sup>-MMT unit cell (1x1x1) at 300K (continued)

P(GPa)	Velocity of sound									Lame constants	
	X1	Y1	Z1	X2	Y2	Z2	X3	Y3	Z3	$\lambda$	$\mu$
0.0001	3.1553	3.1369	3.1929	4.5669	4.6146	3.2545	7.9289	7.9878	5.7599	81.3431	44.674
0.2	3.2134	3.2419	3.2943	4.5909	4.6318	3.3163	8.0764	8.0345	5.85	83.234	46.128
0.4	3.1835	3.2728	3.2804	4.5754	4.6309	3.3523	7.8754	8.1123	5.9129	82.1139	46.2476
0.8	3.138	3.3565	3.2708	4.5689	4.6107	3.4206	8.1259	8.1724	6.0188	88.2057	46.7877
1	3.3365	3.2844	3.3452	4.5764	4.6143	3.413	8.0895	8.1155	6.0333	86.0224	47.3881
1.6	3.3713	3.3848	3.4357	4.5522	4.5909	3.4452	8.0697	8.1935	6.1622	88.0649	48.3273
3	3.5351	3.565	3.6083	4.6367	4.678	3.6255	8.5313	8.5612	6.4572	101.287	52.5549
6	3.7769	3.7898	3.8252	4.6988	4.7416	3.8503	8.814	8.9343	7.0772	117.448	58.2044
9	3.9613	3.9795	3.9945	4.7896	4.838	4.0565	9.0963	9.2331	7.3596	127.821	63.7529

### 3.5 Exfoliation Studies on Organically Modified-MMT

We displaced  $\text{Na}^+$  with alkyl amine. Dreiding FF for alkyl amine (AA) (organic) [21], MSQ-Clay FF for MMT (inorganic) [22, 25] were chosen for exfoliation study.  $\text{NH}_3\text{C}_n\text{H}_{2n+1}$ -MMT models, where  $n$  is between 1 and 18, have been built to analyze the mechanism of the increase of the gallery height of the organically modified MMT as function of  $n$  (in AA tail).

After the first energy minimization, the quenched dynamics was started in an NVT ensemble at temperatures between 300K and 600K. In anneal dynamics; periods of dynamic simulations are followed by a quench period in which the structure is minimized. A dynamic time step was 0.001 ps. The silicate layers were kept fixed (frozen) during dynamic simulations. The *anneal dynamics* allowing relaxation of parameter  $c$  run for 75 ps (5 cycles of 15ps each) shown in Fig. 24.

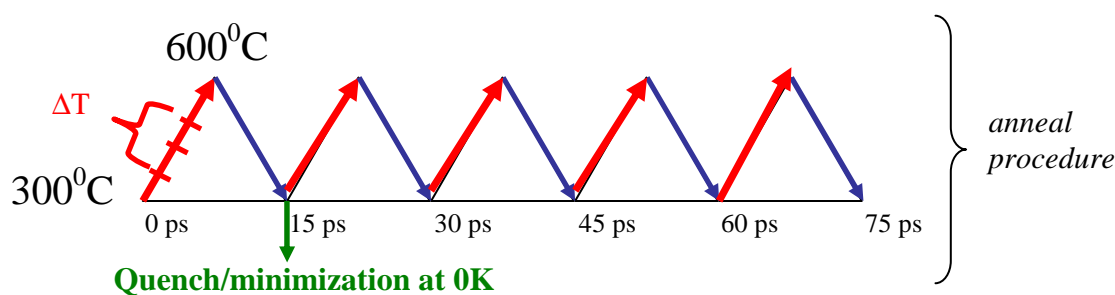


**Fig. 24.** Annealing procedure for alkyl amine-MMT molecular dynamics

As a result, when the number of carbon atoms of the main chains of the alkyl-amines (ammoniums) increases, the gallery height of the alkyl amine-MMTs increases. In our calculations, we confirmed increasing of interlayer distance between the MMT clay sheets, when it is intercalated with methyl, propyl, butyl, and dodecyl ammonium. This argument is shown with numbers in Fig. 25 and Table 10.

**Table 10.** Gallery height changes with respect to various number of carbon atoms and various anneal cycles

n	1	3	4	6	8	10	11	12	14	16	18
<b>5 anneal cycles</b>	11.36	13.18	12.91	13.23	13.88	14.28	17.02	16.99	17.86	17.88	18.15
<b>2:4 anneal cycles</b>	11.27	13.29	12.91	13.29	13.27	13.81	17.18	17.03	18.07	18.09	18.27
<b>experimental [52]</b>	12.88	13.88	13.99					15.89*			

\*This experimental result is for bilayered AA-MMT where  $n=12$

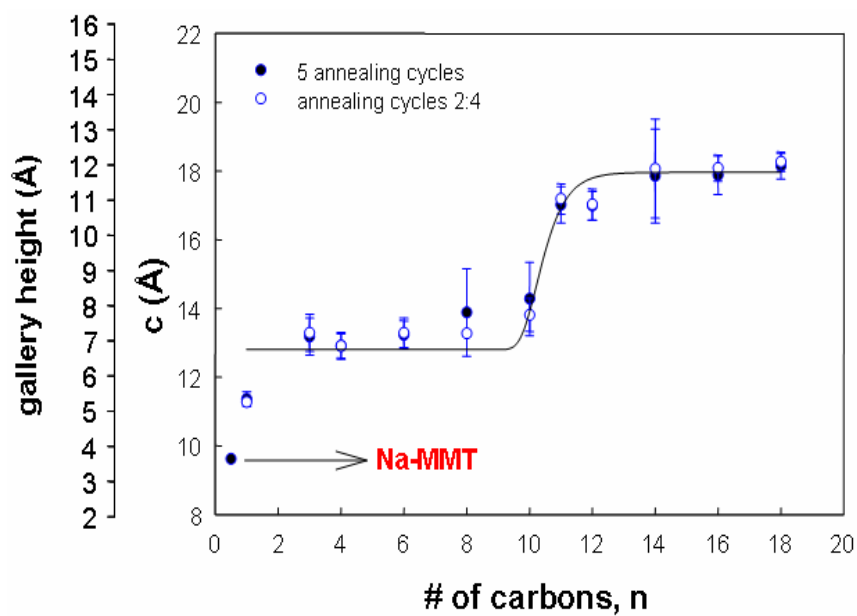


**Fig. 25.** Gallery height versus number of carbons  $n$  in the AA tail average at  $300^{\circ}\text{C}$

### 3.6 VASP Calculations

The calculation was carried out using projector augmented wave (PAW) potentials. The Monkhorst-Pack scheme was used with  $2 \times 2 \times 2$  mesh specifications to sample out the Brillouin zone.

For plane wave density functional theory codes, energy cut-off value must be chosen for the desired accuracy. We performed some bulk calculations with different energy cut-off to find out the energy cut-off. In bulk calculations, the energy cutoff convergence for the plane wave expansion of the wave function chosen as 1000 eV (Fig. 26). After choosing the cut-off energy for  $\text{Na}^+$ -MMT unit cell ( $1 \times 1 \times 1$ ), the cut-off energy for the plane waves was calculated as 1000 eV, and  $2 \times 2 \times 2$  k-mesh was used for all calculations.

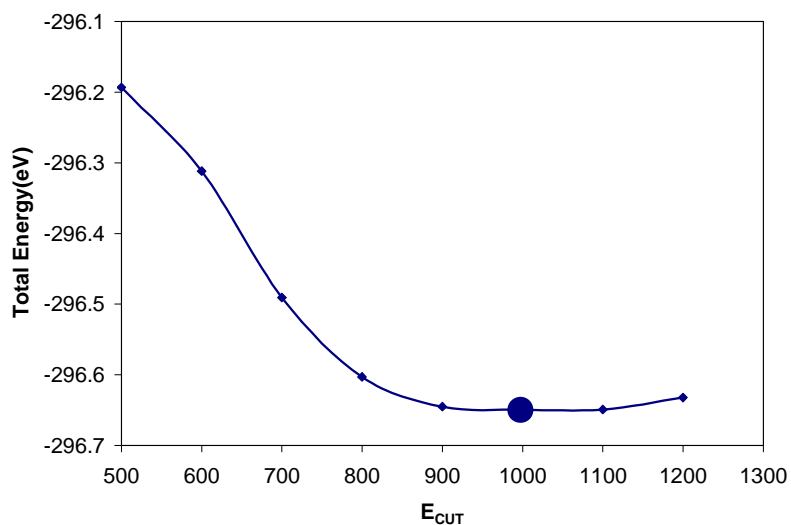


**Fig. 26.** Determination of cut off energy value for  $\text{Na}^+$ -MMT unit cell ( $1 \times 1 \times 1$ ) by using VASP

The stress tensor and the force are always calculated for various options. In our experimental structure data calculations, we used no cell parameter and volume changes in Option 1. In Option 2, cell parameters and volume changes are allowed during

calculations. Cell parameters and ion movement are allowed at constant volume in Option 3. After that, we compared the other theoretical calculations with experimental results. In Table 11, RMS coordinate difference is equal to “0” because Option 4 does not include relaxation ion. root mean square (RMS) coordinate differences are calculated by using difference between calculated theoretical coordinates and experimental coordinates from X-ray diffraction shown in Eq. 46.

$$RMS\ coordinate\ difference = \sqrt{\frac{\sum_{i=1}^N (X_{exp} - X_{theo})_i^2 + (Y_{exp} - Y_{theo})_i^2 + (Z_{exp} - Z_{theo})_i^2}{N-1}} \quad (46)$$

**Table 11.** Na<sup>+</sup>-MMT unit cell shape and volume optimization

<b>Option #</b>	<b>RMS coordinate difference</b>	<b>%error for cell parameters</b>	<b>%error for volume</b>
1	0.203	0	0
2	0.197	3.11	8.8
3	0.202	1.15	0
4	0	0.21	0

Experimental and theoretical cell parameters are compared by using cell shape and volume optimization and RMS coordinate difference is calculated for variation of cell parameters. In our calculations, we calculated RMS is around 0.2 Å. This means that our theoretical calculations give very close results for comparing of experimental data.

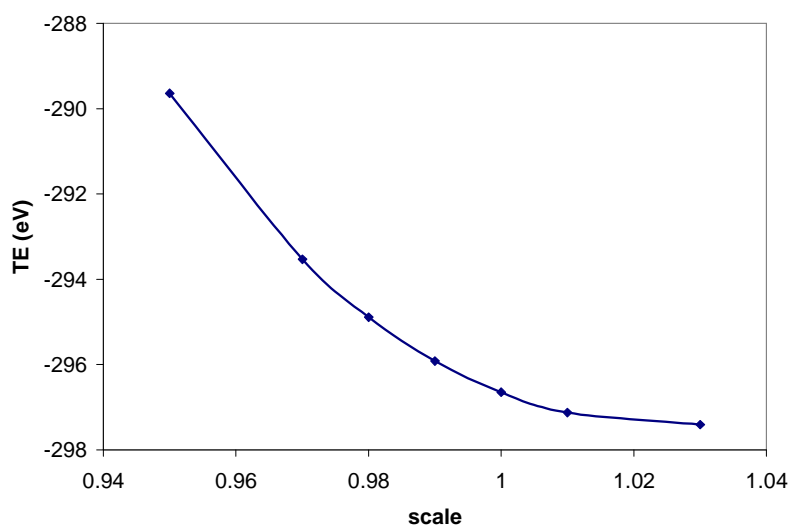


**Fig. 27.** Total energy changes for Na<sup>+</sup>-MMT unit cell (1x1x1) by using volume optimization method in VASP

Cell parameters and volume changes are allowed during volume optimization. We tried to compress and expand the system for optimizing our structure. We used a scale that is equal to proportion of assumed volume to initial volume. When we plot the results,  $1.03 \cdot V_0$  gives the lowest energy that system needs (Fig. 27). Fig. 28 shows that system energy changes with respect to pressure. Compression of the structure will increase the cost of energy and nonetheless these results explain the strength of Na<sup>+</sup>-MMT structure.

When we optimized the cell parameter  $c$ , we have reached  $-0.5 \cdot c_0$  gives us the optimum theoretical result which is similar with X-ray diffraction data shown in Table 12. For minimum cost of energy, we can compress parameter  $c$  up to  $0.5 \cdot c_0$ .



**Table 12.** Optimization of cell parameter  $c$  and RMS results for  $\text{Na}^+$ -MMT unit cell (1x1x1) by using volume optimization method in VASP

scale for $c$ parameter	RMS
<b>-0.5</b>	<b>0.264</b>
0.5	0.401
1	0.396
1.5	0.3962

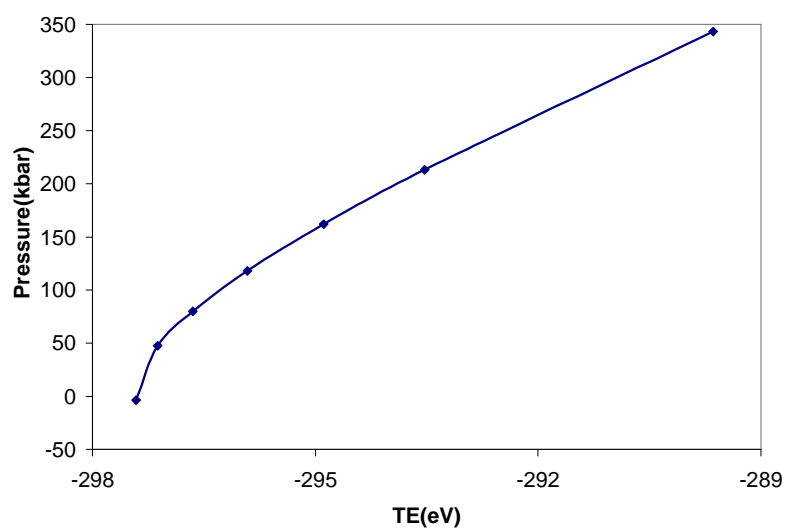


**Fig. 28.** Pressure and total energy changes for  $\text{Na}^+$ -MMT unit cell (1x1x1) during volume optimization in VASP

## CHAPTER IV

### CONCLUSION

In this molecular dynamics study, we have started to worked on calculations of thermodynamic and mechanical properties of  $\text{Na}^+$ -MMT. One of the first steps to be pursued in molecular modeling is the defining a force field that contains parameters that proper characterize the physical interactions between the component atoms that form the model. We selected the Morse-Stretch Charge Equilibration Force Field (MSQ) for the inorganic clay structure [20] and the Dreiding Force Field for the organic alkyl amine component [21] to model nanocomposites during our research studies. We have compared our calculated thermodynamic properties that are very favorably with experimental data.

In second part of this study, we have defined the exfoliation energetics for entropic contribution of  $\text{Na}^+$ -MMT layered structures. Required energy in various layered structures for exfoliation depends on temperature changes because of entropic contribution of the system changes. We have realized that there is more entropic contribution for thinner nanolayers to exist.

In third part of our molecular dynamics study, we investigate the effect of a variable number of carbon atoms (n) in the alkyl-ammonium tail on the interlayer distance. We realized that the gallery height between the alkyl amine and MMT sheets increased with increasing number of carbon atoms in the alkyl-amine for intercalation. Our calculations point out that there is a transition from monolayer to bi-layer of the confined alkyl-amine chains when n increases from 10 to 12.

In the last part of our simulation calculations, we have investigated structural properties of  $\text{Na}^+$ -MMT with density functional theory (DFT) at gap level. We compared crystal XRD data with our results favorably by using RMS calculation method. We optimized the cell shape and volume for  $\text{Na}^+$ -MMT crystal structure by using VASP simulation program.

We did all our computational experiments in nanoscale. After all these calculations, we need to adapt our clay nanocomposite material to macroscale for industrial applications and compare its mechanical and physical properties with other optimization techniques.

In future work, we are planning to optimize nanocomposite systems for producing minimal weight productions and primarily satisfying the specified stress, and displacement criteria. Yet, these are sorted in three main groups [53].

*1. Sizing Optimization:* Design parameters are the sizing parameters associated with the finite-element model such as the cross-sectional areas of the nanocomposites [54]. These areas might be considered to be continuous or discrete variables. There are quite few works have been done on continuous members and continuous search domains by using the means of traditional optimizations techniques. Members having distinct shapes, independent values of area and inertia relative to other members are called discrete members. With the assistance of modern heuristic techniques, it is possible to perform optimization investigations on discrete members.

*2. Geometry Optimization:* By changing the loads and displacement between the layers another design parameter shape is characterized.

*3. Topology Optimization:* This refers to the placement of the different cations or polymer and distance between layers. Along with this, topology optimization also governs the number of layers that actually exist in the structure along with their support conditions.

Finally, in future, we are planning to develop a new model for exfoliation kinetics. We want to construct a new nanocomposite material with designed properties by using experimental and theoretical molecular dynamic methods. Our aim is modeling and production of a new nanocomposite material which will be a cheap, lightweight and widely used material.

## REFERENCES

- [1] M. I. Matar, Ph.D. Dissertation, North Dakota State University, Fargo, 2005.
- [2] X. Zheng, Ph.D. Dissertation, Marquette University, Milwaukee, 2005.
- [3] Colgate University, <http://classes.colgate.edu/rapril/geol201/summaries/silicates/-images/tot.jpg>, (accessed on November, 2006)
- [4] READE Advanced Materials, <http://www.reade.com/Products/Minerals-and-Ores/Montmorillonite-%10-Smectite.html> (accessed on December, 2006)
- [5] California Earth Minerals, Corp., [http://www.the-vu.com/edible\\_clay.htm](http://www.the-vu.com/edible_clay.htm) (accessed on November, 2006)
- [6] S. Lei, Ph.D. Dissertation, Concordia University, Montreal, Canada, 2004.
- [7] T. J. Pinnavaia, G. W. Beall, Polymer-clay Nanocomposites, John Wiley, Chichester, England, 2000.
- [8] C. O. Oriakhi, Chemistry in Britain 34 (1998) 59-62.
- [9] O. C. Wilson Jr, T. Olorunyolemi, A. Jaworski, L. Borum, D. Young, A. Siritwat, E. Dickens, C. Oriakhi, M. Lerner, Applied Clay Science 15 (1999) 265-279.
- [10] C. O. Oriakhi, I. V. Farr, M. M. Lerner, Clays and Clay Minerals 45 (1997) 194-202.
- [11] M. Alexandre, P. Dubois, Materials Science and Engineering: R: Reports 28 (2000) 1-63.
- [12] J. Denault, B. Labrecque, Technology Group on Polymer Nanocomposites in: P.-T. I. M. Institute (Ed.) National Research Council Canada, Boucherville, Québec, 2004, p. J4B 6Y4.

- [13] D. Frenkel, B. Smit, *Understanding Molecular Simulation - From Algorithms to Applications*, Academic Press, California, 2002.
- [14] A. Gonis, *Theoretical Materials Science: Tracing the Electronic Origins of Materials Behavior*, Material Research Society, Warrendale, Pa., 2000, p. 1031.
- [15] M. P. Allen, D. J. Tildesley, *Computer Simulation of Liquids*, Clarendon Press, Oxford, 1987.
- [16] B. J. Alder, T. E. Wainwright, *The Journal of Chemical Physics* 27 (1957) 1208-1209.
- [17] A. Rahman, *Physical Review* 136 (1964) A405.
- [18] J. R. Maple, U. Dinur, A. T. Hagler, *Proceedings of the National Academy of Science* 85 (1988) 5350-5354.
- [19] J. Wang, R. M. Wolf, J. W. Caldwell, P. A. Kollman, D. A. Case, *Journal of Computational Chemistry* 25 (2004) 1157-1174.
- [20] E. Demiralp, T. Çagin, W. A. Goddard, *Physical Review Letters* 82 (1999) 1708.
- [21] S. L. Mayo, B. D. Olafson, W. A. Goddard, *Journal of Physical Chemistry* 94 (1990) 8897-8909.
- [22] A. K. Rappe, W. A. Goddard, *Journal of Physical Chemistry* 95 (1991) 3358 - 3363.
- [23] S. B. Sane, T. Çagin, W. G. Knauss, I. W. A. Goddard, *Journal of Computer-Aided Materials Design* 8 (2001) 87-106.
- [24] C. F. Fan, T. Cagin, Z. M. Chen, *Macromolecules* 27 (1994) 2383 - 2391.
- [25] E. Demiralp, T. Cagin, W. A. Goddard, *Physical Review Letters* 82 (1999) 1708.

- [26] N. T. Huff, E. Demiralp, T. Cagin, W. A. Goddard Iii, *Journal of Non-Crystalline Solids* 253 (1999) 133-142.
- [27] S. Hwang, M. Blanco, E. Demiralp, T. Cagin, W. A. Goddard, *J. Phys. Chem. B* 105 (2001) 4122-4127.
- [28] O. Kitao, E. Demiralp, T. Cagin, S. Dasgupta, M. Mikami, K. Tanabe, W. A. Goddard Iii, *Computational Materials Science* 14 (1999) 135-137.
- [29] S.-N. Luo, T. Cagin, A. Strachan, W. A. Goddard, T. J. Ahrens, *Earth and Planetary Science Letters* 202 (2002) 147-157.
- [30] Wikipedia, Statistical ensemble (mathematical physics), [http://en.wikipedia.org/wiki/Statistical\\_ensemble](http://en.wikipedia.org/wiki/Statistical_ensemble) (accessed on October, 2006)
- [31] K. Han, Ph.D. Dissertation, Texas A&M University, College Station, 2006.
- [32] T. Liang, Ph.D. Dissertation, The Ohio State University, 2005.
- [33] A. Gonis, *Theoretical Materials Science: Tracing the Electronic Origins of Materials Behavior*, Material Research Society, Warrendale, Pa., 1945, p. xiv, 1025
- [34] N. W. Ashcroft, N. D. Mermin., *Solid State Physics* Holt, Rinehart and Winston, New York, 1976, p. xxi, 826 p.
- [35] J. R. Chelikowsky, *Journal of Physics D: Applied Physics* 33 (2000) R33-R50.
- [36] G. Kresse, J. Hafner, *Physical Review B* 47 (1993) 558.
- [37] G. Kresse, J. Furthmüller, *Physical Review B* 54 (1996) 11169.
- [38] M. T. Yin, M. L. Cohen, *Physical Review B* 26 (1982) 3259.

- [39] P. Giannozzi, S. de Gironcoli, P. Pavone, S. Baroni, *Physical Review B* 43 (1991) 7231.
- [40] A. F. Voter, F. Montalenti, T. C. Germann, *Annual Review of Materials Research* 32 (2002) 321-346.
- [41] G. Henkelman, H. Jonsson, *The Journal of Chemical Physics* 113 (2000) 9978-9985.
- [42] G. Henkelman, B. P. Uberuaga, H. Jonsson, *The Journal of Chemical Physics* 113 (2000) 9901-9904.
- [43] T. Çagin, J. R. Ray, *Physical Review A* 37 (1988) 247.
- [44] T. Cagin, J. R. Ray, *Physical Review A* 37 (1988) 4510.
- [45] C. F. Fan, S. L. Hsu, *Macromolecules* 25 (1992) 266 - 270.
- [46] Z. Klika, H. Weissmannova, P. Capkova, M. Pospisil, *Journal of Colloid and Interface Science* 275 (2004) 243-250.
- [47] Q. H. Zeng, A. B. Yu, G. Q. Lu, R. K. Standish, *Chem. Mater.* 15 (2003) 4732-4738.
- [48] S. I. Tsipursky, V. A. Drits, *Clay Minerals* 19 (1984) 177-193.
- [49] R. Toth, A. Coslanich, M. Ferrone, M. Fermeglia, S. Pricl, S. Miertus, E. Chiellini, *Polymer* 45 (2004) 8075-8083.
- [50] Y. Yang, Z.-k. Zhu, J. Yin, X.-y. Wang, Z.-e. Qi, *Polymer* 40 (1999) 4407-4414.
- [51] T. D. Fornes, D. R. Paul, *Polymer* 44 (2003) 4993-5013.

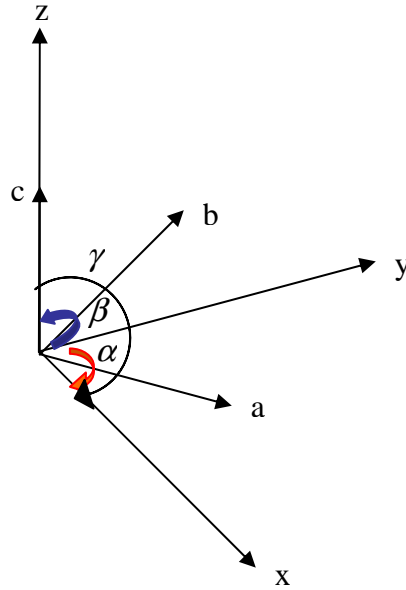
[52] P. Bala, B. K. Samantaraya, S. K. Srivastava, *Materials Research Bulletin* 35 (2000) 1717-1724.

[53] P. Agarwal, Ph.D. Dissertation, Texas A&M University, College Station, 2006

[54] S. D. Rajan, *Journal of Structural Engineering* 121 (1995) 1480-1487.



## APPENDIX A



The cell vectors  $\vec{a}$ ,  $\vec{b}$  and  $\vec{c}$  coincide with Cartesian axes x, y, z and atomic positions are given in XYZ direction so they are converted to abc direction as  $\vec{\xi}, \vec{\eta}, \vec{\zeta}$ .  $\vec{a}$ ,  $\vec{b}$  and  $\vec{c}$  are given in Table 5 and atomic positions  $(\vec{\xi}, \vec{\eta}, \vec{\zeta})$  are shown Table 6.

$$\vec{H} = \vec{H} = \begin{pmatrix} \vec{a} \\ \vec{b} \\ \vec{c} \end{pmatrix}$$

$$\mathbf{H} = \begin{bmatrix} a_x & 0 & 0 \\ a_y & b_y & 0 \\ a_z & b_z & c_z \end{bmatrix} \text{ where } \begin{aligned} a_x &= a \sin \beta \sin \gamma^* \\ a_y &= a \sin \beta \cos \gamma^*; & b_y &= b \sin \alpha \\ a_z &= a \cos \beta & ; & b_z = b \cos \alpha \end{aligned}$$

$$\text{where } \cos \gamma^* = \frac{(\cos \gamma - \cos \alpha \cos \beta)}{\sin \alpha \sin \beta}$$

$$\vec{R} = \vec{R} = (\vec{\xi}, \vec{\eta}, \vec{\zeta})$$

$$\vec{\rho} = \vec{\rho} = (x, y, z)$$

$$\mathbf{R} = \mathbf{H} \boldsymbol{\rho}$$

$$\begin{bmatrix} x \\ y \\ z \end{bmatrix} = \begin{bmatrix} a_x & 0 & 0 \\ a_y & b_y & 0 \\ a_z & b_z & c_z \end{bmatrix} \begin{bmatrix} \xi \\ \eta \\ \zeta \end{bmatrix}$$

## APPENDIX B

VERSION	
CERIUS2	1
END	
#	
HEADER	
END	
#	
PREFERENCES	
BONDS	T
ANGLES	T
COULOMB	T
INVERSIONS	T
TORSIONS	T
UREY_BRADLEY	F
STRETCH_STRETCH	F
SEPARATED_STRETCH_STRETCH	F
STRETCH_BEND_STRETCH	F
BEND_BEND	F
TORSION_STRETCH	F
TORSION_BEND_BEND	F
BEND_TORSION_BEND	F
STRETCH_TORSION_STRETCH	F
HYDROGEN_BONDS	F
DIAGONAL_VAN_DER_WAALS	T
OFF_DIAGONAL_VAN_DER_WAALS	T
IGNORE_UNDEFINED_TERMS	T
NON-BONDED_3-BODY	F
SHRINK_CH_BONDS	F
SHRINK_CH_H_ATOM	H_C
SHRINK_CH_FACTOR	0.915
SINGLE_TORSION	F
SCALE_TORSIONS_ABOUT_COMMON_BOND	T
SCALE_BY_N_DEFINED_TORSIONS	T
EXOCYCLIC_TORSIONS_SCALE_FACTOR	0.4

SINGLE_INVERSION	F
H-BOND_METHOD	SPLINE
H-BOND_LIST	T
H-BOND_DIRECT_RCUT	4
H-BOND_SPLINE_DISTANCE_ON	4
H-BOND_SPLINE_DISTANCE_OFF	4.5
H-BOND_SPLINE_ANGLE_ON	65
H-BOND_SPLINE_ANGLE_OFF	75
H-BOND_LIST_DISTANCE_OFF	6.5
H-BOND_LIST_ANGLE_OFF	90
NB_NEIGHBOUR_SEARCH_METHOD	LIST
NON_BOND_BUFFER_DISTANCE	2
H-BOND_BUFFER_DISTANCE	2
COU_DIELECTRIC_CONSTANT	1
COU_INTER_CUT_OFF	8.5
COU_SPLINE_OFF	16.5
COU_SPLINE_ON	16
EWALD_SUM_COU_ACCURACY	0.001
EWALD_SUM_COU_ETA	4.822
EWALD_SUM_COU_KCUT	0.269
EWALD_SUM_COU_RCUT	16.22
EWALD_SUM_COU_OPTIMIZE	SMART
COU_EXCLUDE_1-2	T
COU_EXCLUDE_1-3	T
COU_EXCLUDE_1-4	F
COU_1-4_SCALE_FACTOR	1
COU_METHOD	EWALD
COU_DIRECT_CUT-OFF	16
VDW_COMBINATION_RULE	GEOMETRIC
VDW_INTER_CUT_OFF	8.5
VDW_EXCLUDE_1-2	T
VDW_EXCLUDE_1-3	T
VDW_EXCLUDE_1-4	F
VDW_1-4_SCALE_FACTOR	1
VDW_METHOD	EWALD
VDW_SPLINE_ON	16
VDW_SPLINE_OFF	16.5

EWALD_SUM_VDW_OPTIMIZE	SMART
EWALD_SUM_VDW_ACCURACY	0.00100
EWALD_SUM_VDW_ETA	2.86800
EWALD_SUM_VDW_KCUT	0.40621
EWALD_SUM_VDW_RCUT	8.43629
EWALD_SUM_VDW_REP_CUT	7.35834
FAST_EWALD_SUM_RATIO	10
SLOW_EWALD_SUM_RATIO	5
MINIMUM_IMAGE	F
ASSIGN_MASS	T
ASSIGN_CHARGE	F
ASSIGN_HYBRIDIZATION	T
ASSIGN_VALBOND_CENTER	F
ATOM_TYPE	F
ATOM_TYPE_ALL	T
CALCULATE_BOND_ORDER	F

END

#

ATOMTYPES

H_C	H	1.0080	0	0	0	0
O_3C	O	15.9994	0	3	0	2
O_AC	O	15.9994	0	3	0	2
Al3C	Al	26.9815	0	3	0	0
Si3C	Si	28.0860	0	3	0	0
H_	H	1.0080	0	0	0	0
C_3	C	12.0110	0	3	0	0
N_3	N	14.0067	0	3	0	1
O_3	O	15.9994	0	3	0	2
O_w	O	15.9994	-0.82	2	0	0
H_w	H	1.0080	0.41	2	0	0
K_C	K	39.1000	1	0	0	0
Na_C	Na	22.9900	1	0	0	0
Mg_C	Mg	24.3100	0	3	0	0
Ca_C	Ca	40.0800	0	6	0	0
C_R	C	12.0110	0	2	0	0
N_R	N	14.0067	0	2	0	1

END

#

## DIAGONAL\_VDW

H_C	VDW_MORSE	3.3472	3.8E-05	12
O_3C	VDW_MORSE	3.7835	0.5363	10.4112
O_AC	VDW_MORSE	3.7835	0.5363	10.4112
Al3C	VDW_MORSE	3.8915	0.3321	11.9071
Si3C	VDW_MORSE	3.4103	0.2956	11.7139
H_	EXPO_6	3.1950	0.0152	12.3820
C_3	EXPO_6	3.8983	0.0951	14.0340
N_3	EXPO_6	3.6621	0.0774	13.8430
O_3	EXPO_6	3.4046	0.0957	13.4830
O_w	LJ_6_12	3.5532	0.1848	
H_w	LJ_6_12	0.9000	1.0000	
K_C	VDW_MORSE	2.8595	0.3440	13.8000
Na_C	VDW_MORSE	2.8595	0.3440	13.8000
Mg_C	VDW_MORSE	3.9109	0.4018	11.1758
Ca_C	VDW_MORSE	3.8305	0.7148	14.1651
C_R				
LJ_6_12	3.8983	0.0951		
N_R				
LJ_6_12	3.6621	0.0774		

END

#

#

## ATOM\_TYPING\_RULES

Si3C	Si	3	0	0	1
Al3C	Al	3	0	0	1
O_w	O	3	0	2	1
	H	0	0	0	1
	H	0	0	0	1
H_w	H	0	0	1	1
	O	3	0	2	1
	H	0	0	0	1
	H	0	0	0	1
Mg_C	Mg	0	0	0	-1
Ca_C	Ca	0	0	0	0
K_C	K	0	0	0	1
Na_C	Na	0	0	0	1
C_3	C	3	0	0	1

C_R	C	2	0	1	1
	**	2	0	2	1
	**	2	0	0	1
	**	2	0	0	1
C_R	C	2	0	1	1
	**	2	0	2	1
	**	2	0	0	1
	O	3	0	0	1
C_R	C	2	0	2	1
	**	2	0	0	1
	**	2	0	0	1
C_R	C	2	0	2	1
	**	2	0	0	1
	O	3	0	0	1
N_3	N	3	0	0	1
N_R	N	2	0	1	1
	**	2	0	2	1
	**	2	0	0	1
N_R	N	2	0	1	1
	**	2	0	2	1
	**	2	0	0	1
	O	3	0	0	1
N_R	N	2	0	2	1
	**	2	0	0	1
	**	2	0	0	1
N_R	N	2	0	2	1
	**	2	0	0	1
	O	3	0	0	1
H_C	H	0	0	1	1
	O	3	0	1	1
	Al	0	0	0	-1
O_AC	O	3	0	1	1
	Si	0	0	0	1
O_3C	O	3	0	1	1
	H	0	0	0	1
O_3C	O	3	0	1	1
	Al	0	0	0	-1

H_	H	0	0	1	1
	C	3	0	0	1
H_	H	0	0	1	1
	C	2	0	0	1
H_	H	0	0	1	1
	N	0	0	1	1
	C	0	0	0	1

END

#

#

## OFF\_DIAGONAL\_VDW

O_3C	H_C	VDW_MORSE	1.0770	19.5500	8.4394	P*
O_AC	H_C	VDW_MORSE	2.1768	0.1753	16.0000	P*
O_AC	O_3C	VDW_MORSE	3.7835	0.5363	10.4112	P*
Al3C	O_3C	VDW_MORSE	1.7775	26.0300	9.7830	P*
Al3C	O_AC	VDW_MORSE	1.7775	26.0300	9.7830	P*
Si3C	O_3C	VDW_MORSE	1.6248	46.0000	8.3022	P*
Si3C	O_AC	VDW_MORSE	1.6248	46.0000	8.3022	P*
Si3C	Al3C	VDW_MORSE	4.0949	0.0000	8.7732	P*
Ca_C	O_3C	VDW_MORSE	2.4562	4.8296	10.8791	P*
Ca_C	O_3	VDW_MORSE	2.4562	4.8296	10.8791	P*
Ca_C	Na_C	VDW_MORSE	3.4703	0.5978	12.0000	P*
Ca_C	Al3C	VDW_MORSE	4.1007	0.4707	12.0000	P*
Ca_C	Si3C	VDW_MORSE	4.0443	0.4707	12.0000	P*
Ca_C	O_AC	VDW_MORSE	2.4562	4.8296	10.8791	P*
Ca_C	H_	VDW_MORSE	3.4983	0.1042	12.0000	P*
Ca_C	C_3	VDW_MORSE	3.8643	0.2607	12.0000	P*
Ca_C	N_3	VDW_MORSE	3.7454	0.2352	12.0000	P*
Ca_C	O_w	VDW_MORSE	3.6615	0.2071	12.0000	P*
Ca_C	H_w	VDW_MORSE	3.4983	0.0003	12.0000	P*
H_	H_C	EXPO_6	3.1950	0.0152	12.3820	P*
H_	O_3C	EXPO_6	3.3043	0.0378	12.9456	P*
H_	O_AC	EXPO_6	3.3043	0.0378	12.9456	P*
H_	Al3C	EXPO_6	3.6245	0.0821	11.9769	P*
H_	Si3C	EXPO_6	3.5927	0.0799	12.0101	P*
C_3	H_C	EXPO_6	3.5392	0.0376	13.2285	P*
C_3	O_3C	EXPO_6	3.6368	0.0964	13.7475	P*
C_3	O_AC	EXPO_6	3.6368	0.0964	13.7475	P*
C_3	Al3C	EXPO_6	4.0863	0.1853	12.9405	P*
C_3	Si3C	EXPO_6	4.0447	0.1816	12.9640	P*
N_3	H_C	EXPO_6	3.4315	0.0338	13.1348	P*
N_3	O_3C	EXPO_6	3.5298	0.0862	13.6609	P*



N_3	O_AC	EXPO_6	3.5298	0.0862	13.6609	P*
N_3	Al3C	EXPO_6	3.9267	0.1751	12.7884	P*
N_3	Si3C	EXPO_6	3.8895	0.1709	12.8166	P*
O_3	H_C	EXPO_6	3.3043	0.0378	12.9456	P*
O_3	O_3C	EXPO_6	3.4046	0.0957	13.4830	P*
O_3	O_AC	EXPO_6	3.4046	0.0957	13.4830	P*
O_3	Al3C	EXPO_6	3.7463	0.2059	12.5384	P*
O_3	Si3C	EXPO_6	3.7136	0.2002	12.5716	P*
O_w	H_C	EXPO_6	3.3043	0.0378	12.9456	P*
O_w	O_3C	EXPO_6	3.4046	0.0957	13.4830	P*
O_w	O_AC	EXPO_6	3.4046	0.0957	13.4830	P*
O_w	Al3C	EXPO_6	3.7463	0.2059	12.5384	P*
O_w	Si3C	EXPO_6	3.7136	0.2002	12.5716	P*
H_w	H_C	EXPO_6	3.1950	0.0152	12.3820	P*
H_w	O_3C	EXPO_6	3.3043	0.0378	12.9456	P*
H_w	O_AC	EXPO_6	3.3043	0.0378	12.9456	P*
H_w	Al3C	EXPO_6	3.6245	0.0821	11.9769	P*
H_w	Si3C	EXPO_6	3.5927	0.0799	12.0101	P*
Na_C	O_3C	VDW_MORSE	2.9105	0.2604	14.7296	P*
Na_C	H_	VDW_MORSE	3.0226	0.0723	12.0000	P*
Na_C	C_3	VDW_MORSE	3.3387	0.1809	12.0000	P*
Na_C	N_3	VDW_MORSE	3.2360	0.1632	12.0000	P*
Na_C	O_3	VDW_MORSE	2.9105	0.2604	14.7296	P*
Na_C	O_w	VDW_MORSE	3.1636	0.1437	12.0000	P*
Na_C	H_w	VDW_MORSE	3.0226	0.0002	12.0000	P*
Mg_C	O_AC	VDW_MORSE	1.9819	10.6250	12.9104	P*
Mg_C	O_3C	VDW_MORSE	1.9819	10.6250	12.9104	P*
Mg_C	Al3C	VDW_MORSE	4.0949	0.0000	8.7732	P*
Mg_C	Si3C	VDW_MORSE	4.0949	0.0000	8.7732	P*
Mg_C	H_	VDW_MORSE	3.5349	0.0782	12.0000	P*
Mg_C	C_3	VDW_MORSE	3.9046	0.1955	12.0000	P*
Mg_C	N_3	VDW_MORSE	3.7845	0.1764	12.0000	P*
Mg_C	O_3	VDW_MORSE	1.9819	10.6250	12.9104	P*
Mg_C	O_w	VDW_MORSE	3.6997	0.1553	12.0000	P*
Mg_C	H_w	VDW_MORSE	3.5349	0.0002	12.0000	P*
Mg_C	Ca_C	VDW_MORSE	3.6460	0.3093	12.0000	P*
Mg_C	Na_C	VDW_MORSE	3.5065	0.4483	12.0000	P*
C_R	O_3C	VDW_MORSE	3.8443	0.2258	12.0000	P*
C_R	Al3C	VDW_MORSE	3.8949	0.1777	12.0000	P*
C_R	Si3C	VDW_MORSE	3.8284	0.1299	12.0000	P*
C_R	Na_C	VDW_MORSE	3.3387	0.1809	12.0000	P*
C_R	Mg_C	VDW_MORSE	3.9046	0.1955	12.0000	P*
N_R	O_3C	VDW_MORSE	3.7260	0.2037	12.0000	P*

N_R	Al3C	VDW_MORSE	3.7751	0.1603	12.0000	P*
N_R	Si3C	VDW_MORSE	3.7106	0.1172	12.0000	P*
N_R	Na_C	VDW_MORSE	3.2360	0.1632	12.0000	P*
N_R	Mg_C	VDW_MORSE	3.7845	0.1764	12.0000	P*

END  
#  
BOND\_STRETCH

C_3	H_	HARMONIC	700.00	1.090
C_3	C_3	HARMONIC	700.00	1.530
N_3	H_	HARMONIC	700.00	1.022
N_3	C_3	HARMONIC	700.00	1.462
O_3	H_	HARMONIC	700.00	0.980
O_3	C_3	HARMONIC	700.00	1.420
O_3	N_3	HARMONIC	700.00	1.352
H_w	O_w	HARMONIC	500.00	1.000
H_	H_	HARMONIC	700.00	0.650
C_R	H_	HARMONIC	700.00	1.020
C_R	C_3	HARMONIC	700.00	1.460
C_R	C_R	HARMONIC	1050.00	1.390
C_R	N_3	HARMONIC	700.00	1.392
N_3	N_3	HARMONIC	700.00	1.394
N_R	H_	HARMONIC	700.00	0.970
N_R	C_3	HARMONIC	700.00	1.410
N_R	C_R	HARMONIC	1050.00	1.340
N_R	N_3	HARMONIC	700.00	1.342
N_R	N_R	HARMONIC	1050.00	1.290
C_R	O_3	HARMONIC	700.00	1.350
N_R	O_3	HARMONIC	700.00	1.300
O_3C	H_C	HARMONIC	700.00	0.980

END  
#  
ANGLE\_BEND

X	C_3	X	THETA_HARM	100	109.47
X	N_3	X	THETA_HARM	100	106.70
X	O_3	X	THETA_HARM	100	104.51
X	C_R	X	THETA_HARM	100	120.00
X	N_R	X	THETA_HARM	100	120.00
H_w	O_w	H_w	THETA_HARM	120	109.47

END

#

TORSIONS

X	C_3	C_3	X	DIHEDRAL	2	3	-1
X	N_3	N_3	X	DIHEDRAL	2	3	-1
X	O_3	C_3	X	DIHEDRAL	2	3	-1
X	O_3	N_3	X	DIHEDRAL	2	3	-1
X	O_3	O_3	X	DIHEDRAL	2	2	-1
X	C_R	C_3	X	DIHEDRAL	2	3	-1
C_R	C_R	C_3	X	DIHEDRAL	1	6	1
N_R	C_R	C_3	X	DIHEDRAL	1	6	1
X	C_R	C_R	X	DIHEDRAL	25	2	1
X	N_3	C_3	X	DIHEDRAL	2	3	-1
X	C_R	N_3	X	DIHEDRAL	2	3	-1
C_R	C_R	N_3	X	DIHEDRAL	1	6	1
N_R	C_R	N_3	X	DIHEDRAL	1	6	1
X	N_R	C_3	X	DIHEDRAL	2	3	-1
C_R	N_R	C_3	X	DIHEDRAL	1	6	1
N_R	N_R	C_3	X	DIHEDRAL	1	6	1
X	N_R	C_R	X	DIHEDRAL	25	2	1
X	N_R	N_3	X	DIHEDRAL	2	3	-1
C_R	N_R	N_3	X	DIHEDRAL	1	6	1
N_R	N_R	N_3	X	DIHEDRAL	1	6	1
X	N_R	N_R	X	DIHEDRAL	25	2	1
X	C_R	O_3	X	DIHEDRAL	2	2	1
X	N_R	O_3	X	DIHEDRAL	2	2	1

END

#

INVERSIONS

N_3	X	X	X	IGNORE		
C_R	X	X	X	UMBRELLA	40	0
N_R	X	X	X	UMBRELLA	40	0

END

#

## HYDROGEN\_BONDS

X	X	LJ_12_10	4	2.75
---	---	----------	---	------

END

#

COULOMBIC

X X CONST-EPS

END

## VITA

Selma Atilhan was born in Balikesir, Turkey on February 7, 1981. She received her Bachelor of Science and Master of Science degrees in chemical engineering from Ege University, Izmir, Turkey. She joined the Department of Chemical Engineering at Texas A&M University in August 2005 as a Master of Science student. Her current research interests include molecular dynamics simulation and its applications to polymer/clay nano-composites. Following graduation, Selma continued her studies at Texas A&M University as a Doctor of Philosophy student in the same department. Her permanent address is:

Ataturk Mh. Bandirma Cd,

Belgin Apt., No:57/7

Balikesir, TURKEY

10100

Selma Atilhan may be reached via e-mail at [selma.atilhan@gmail.com](mailto:selma.atilhan@gmail.com)